

MULTI-COMPONENT GROUND MOTION RESPONSE SPECTRA FOR COUPLED HORIZONTAL, VERTICAL, ANGULAR ACCELERATIONS, AND TILT

Erol Kalkan and Vladimir Graizer

California Geological Survey
Sacramento, CA 95814-3500, U.S.A.

ABSTRACT

Rotational and vertical components of ground motion are almost always ignored in design or in the assessment of structures despite the fact that vertical motion can be twice as much as the horizontal motion and may exceed $2g$ level, and rotational excitation may reach few degrees in the proximity of fault rupture. Coupling of different components of ground excitation may significantly amplify the seismic demand by introducing additional lateral forces and enhanced P- Δ effects. In this paper, a governing equation of motion is postulated to compute the response of a SDOF oscillator under a multi-component excitation. The expanded equation includes secondary P- Δ components associated with the combined impacts of tilt and vertical excitations in addition to the inertial forcing terms due to the angular and translational accelerations. The elastic and inelastic spectral ordinates traditionally generated considering the uniaxial input motion are compared at the end with the multi-component response spectra of coupled horizontal, vertical and tilting motions. The proposed multi-component response spectrum reflects kinematic characteristics of the ground motion that are not identifiable by the conventional spectrum itself, at least for the near-fault region where high intensity vertical shaking and rotational excitation are likely to occur.

KEYWORDS: Rotational Motion, Tilt, Vertical Acceleration, Response Spectrum, P- Δ Effects

BACKGROUND

Ground motion response spectrum is defined as a graphical relationship of the peak response of a single-degree-of-freedom (SDOF) oscillator having certain damping to dynamic motion or forces. Since it was first introduced by Biot (1932, 1933, 1934, 1941, 1942), and later introduced to engineering applications by Housner (1959) and Newmark et al. (1973), it has often been utilized for the purposes of recognizing the significant characteristics of accelerograms and evaluating the response of structures to strong ground shaking in a simple fashion. Due to inherent theoretical simplicity and ease in computer applications, the response spectrum concept quickly became the standard tool of structural design and performance assessment.

Earthquake recordings generally produce jagged spectral response shapes manifesting large record-to-record variability. Due to abrupt changes from maxima to minima over a narrow band of spectral periods, use of a single-record response spectrum in generalizing the seismic demand is generally avoided. Instead, spectra from a suite of ground motions are smoothed, scaled and averaged; thereby inherent variability in ground motion process is statistically accounted for. To be used directly in design, Biot (1941, 1942) and then Housner (1959) were the first to propose a smooth-response spectrum. Later, Newmark and Hall (1969, 1982) followed the same idea. Newmark-Hall's smooth spectrum constituted three regions along the spectral periods: (i) acceleration (short-period range), (ii) velocity (intermediate-period range), and (iii) displacement (long-period range). Each of these regions is constructed by applying dynamic amplifications to the design values of peak ground acceleration (PGA), velocity (PGV) and displacement (PGD). Following Newmark and Hall (1969, 1982), many researchers contributed to the development of the smooth spectrum, e.g., Hall et al. (1975), Mohraz (1976), Seed et al. (1976), Lam et al. (2000), Kalkan and Gülkan (2004a), and Malhotra (2006). A common feature of these studies is that the proposed smooth spectra were developed utilizing a uniaxially excited SDOF oscillator, while contributions of the other ground motion components on translational response were not included.

In reality, earthquakes create movements in three-translational and three-rotational directions; hence the exact response at a point on the ground surface during an earthquake can only be obtained by recording the motions of all six degrees of freedom (DOF). Except for some attempts in recent years towards measuring rotational components, it is routine in seismology to record only translational components in three orthogonal directions. Among these three, only two horizontal components have been almost always involved in spectral response computations. This routine is mainly driven by the common perception, which has been long established considering far-fault earthquake recordings, that rotational components of motion are small so as not to add significantly to the seismic loads, and that structures have sufficient overstrength against the vertical component since they have already been designed for the gravitational acceleration. In fact, the importance of vertical component of ground motion in design and performance assessment was addressed long ago (e.g., Chopra, 1966; Lee, 1979). Yet, it received more attention just after the earthquakes in the last 15 years, which provided plethora of data in the near field of earthquake source having significantly higher vertical acceleration than its horizontal counterparts (Niazi and Bozorgnia, 1991; Bozorgnia et al., 1995; Silva, 1997; Kalkan and Gülkan, 2004b). Such near-fault data has eventually changed the misleading assumption that the vertical ground motion can be taken to be two-thirds of the horizontal motion, as postulated earlier by Newmark et al. (1973), and Newmark and Hall (1982). At short periods and near-source distances, vertical component of the ground motion may be noticeably more severe than the horizontal component. A remarkable field evidence of this fact was found in the recent past, during the 1995 Kobe earthquake, when ground vertical acceleration experienced little attenuation from rock-outcrop to the ground surface, as opposed to the horizontal ones, even in potentially liquefiable soils. As a consequence, high vertical seismic inputs to structures were observed, and unusual failures of vertical structural members occurred (JSCE, 1995; Papazoglou and Elnashai, 1996; Uenishi and Sakurai, 2000). Another example of intense vertical acceleration was observed during the aftershock of 1985 Nahanni earthquake in Canada. The aftershock ($M_s = 6.9$) created a peak horizontal acceleration of 1.25g at a station located 8–10 km of the rupture. The peak vertical acceleration (recorded by an analog type accelerograph, SMA-1) got off-scale and exceeded 2g (Weichert et al., 1986).

In recognition of high-intensity vertical shaking in the vicinity of active faults, many studies have been devoted to investigate the detrimental impacts of vertical ground motion on structural systems. Elnashai and Papazoglou (1997) and Ranzo et al. (1999) demonstrated that shear resistance of the vertical members is more sensitive to the vertical excitation, and that shear failure is anticipated when a reduction in the axial contribution to the section shear capacity occurs. In parallel, Salazar and Haldar (2000) emphasized the increased level of axial load and its damaging effects on the performance of columns designed by the beam-column methodology. Similar findings on the eroded shear capacity of columns due to vertical excitation influences were also highlighted by Abdelkareem and Machida (2000), and Diotallevi and Landi (2000). As recently shown by Kunnath et al. (2005), vertical motion may magnify and potentially create reversal of bending moment in longitudinal bridge girders. Widespread phenomenon of bearing failure and deck unseating, as observed during the recent earthquakes, was partially attributed to the destructive impact of vertical motions (Pamuk et al., 2005). Based on a large body of available studies, it is possible to conclude that vertical shaking may escalate the axial column force, cause an increase in the moment and shear demand, and amplify plastic deformation, extend plastic hinge formation and finally diminish the ductility capacity of structural component. In order to include the vertical motion effects in design, recent efforts have considered the development of vertical ground motion spectra by focusing mostly on near-fault accelerograms (e.g., Ambraseys and Simpson, 1996; Elnashai and Papazoglou, 1997; Bozorgnia and Campbell, 2004; Kalkan and Gülkan, 2004b; Malhotra, 2006). These studies have developed vertical ground motion spectra (for the vertical response computed under unidirectional excitation only) and concentrated on its parallel use with the horizontal ground motion spectra.

In addition to translational ground movement in orthogonal directions and relevant studies quantifying its destructive impacts, studies by Bouchon and Aki (1982), Lee and Trifunac (1985), and Castellani and Boffi (1986) indicated that rotational ground motion could also be important in the near-field zone. Stratta and Griswold (1976), Ghafory-Ashtiany and Singh (1986), and Gupta and Trifunac (1990, 1991) emphasized possible effects of a rotational component on building response. Recently, Graizer (2006a) demonstrated that static tilting of the ground surface could reach a few degrees while dynamic tilting becomes even higher in the proximity of earthquake faults. Such high-intensity ground

tilting becomes detrimental for structures by compelling them to high ductility demand levels (Kalkan and Graizer, 2007).

RESEARCH SIGNIFICANCE

In majority of the past studies, SDOF oscillators were used to compute the response spectra for horizontal and vertical motions separately, assuming that the response to multi-component excitations is uncoupled. However, coupling of different components of ground motion (i.e., concurrent application of different components in computing the SDOF oscillator's response) may significantly amplify the level of seismic demand by producing additional lateral forces and enhanced P- Δ effects without violating the SDOF assumption (i.e., unidirectional response is still valid, while the input is multi-directional). In order to quantify the level of increase in seismic demand, a complete equation of motion for the translational response of a SDOF oscillator is postulated here. The new formulation includes the combined effects of tilt and vertical excitations as the secondary P- Δ components, in addition to the inertial force effects due to the angular and translational accelerations. The inelastic response of a SDOF oscillator to uniaxial input motion and also its response to a three-degree-of-freedom (i.e., horizontal, vertical and rotation) motion are systematically compared and contrasted to isolate the relative contribution of each input motion. The results of this study confirm that higher ductility demand (or dynamic collapse) may ensue due to the effects of vertical and rotational motions when they are coupled with the horizontal excitation. Unlike the conventional spectrum, the proposed multi-component response spectrum (elastic or inelastic) is capable of capturing the enhanced seismic demands associated with multi-component coupling effects.

VERTICAL AND ROTATIONAL GROUND MOTIONS

Prior to investigating the impacts of vertical and rotational (i.e., tilt) components of ground motion on the SDOF oscillator's response, it is instructive first to highlight the fundamental characteristics of the ground motion components. In reviewing the following sections, it should be kept in mind that pendulums (which represent a typical SDOF system) used in strong motion recording instruments are sensitive not only to the horizontal ground shaking, but also to the tilt (i.e., rotational component).

1. Vertical Component of Ground Motion and V/H Ratio

Vertical component of the strong ground motion is mainly associated with body waves: vertically propagating compressional waves (i.e., P-waves) and horizontally propagating dilatational waves (i.e., S-waves). Compared to the horizontal component, vertical motion may be richer in high-frequency content in the near field of an earthquake fault. As the distance from the source increases, difference in the frequency content between horizontal and vertical components becomes much smaller as a result of faster attenuation of high frequencies with distance, and mixing of horizontal and vertical motions due to nonhomogeneities along the wave path.

A common perception in engineering practice is that intensity of vertical ground motion is lower than that of the horizontal; thereby V/H ratio (i.e., the ratio of vertical to horizontal peak ground acceleration) is assumed to remain less than unity. In order to study the variations of V/H ratio, we performed an analysis on 820 three-component strong ground motion records of significant earthquakes in California. This analysis was later extended to cover more than 1400 records. At first, strong motion data from 18 earthquakes of magnitude higher than 5.0 were studied and it was shown that the distribution of V/H ratio could be best presented on the logarithmic scale with the median ratio of 0.47 (Graizer, 2006b). The median ratio of the V/H ratio varied from 0.29 to 0.69 for different events (see Figure 1, where “++” indicates the median V/H ratio for each specific event). To study the distribution of the V/H ratio, the entire data was split into equal bins having $\log(V/H)$ range of 0.05. It was observed that the largest number of V/H ratios lies within the 0.45–0.50 range having 363 data points. As shown in Figure 2 (which includes 1492 data points), in most cases, amplitude of the vertical component is about twice lower than that of the horizontal component. Data points in Figure 2 are from a mixed dataset of far-field and near-field recordings and yield an average V/H ratio of 0.48.

In order to isolate the possible farther distance effects on the resultant V/H ratio, Figure 3 concentrates on recordings measured within 30 km of the closest fault. This subset includes 240 components of ground motions recorded at 80 stations from worldwide earthquakes, and this data was

extracted from the Next Generation Attenuation (NGA) models database (Power et al., 2006). More details of ground motions in this subset are provided in Table 1.

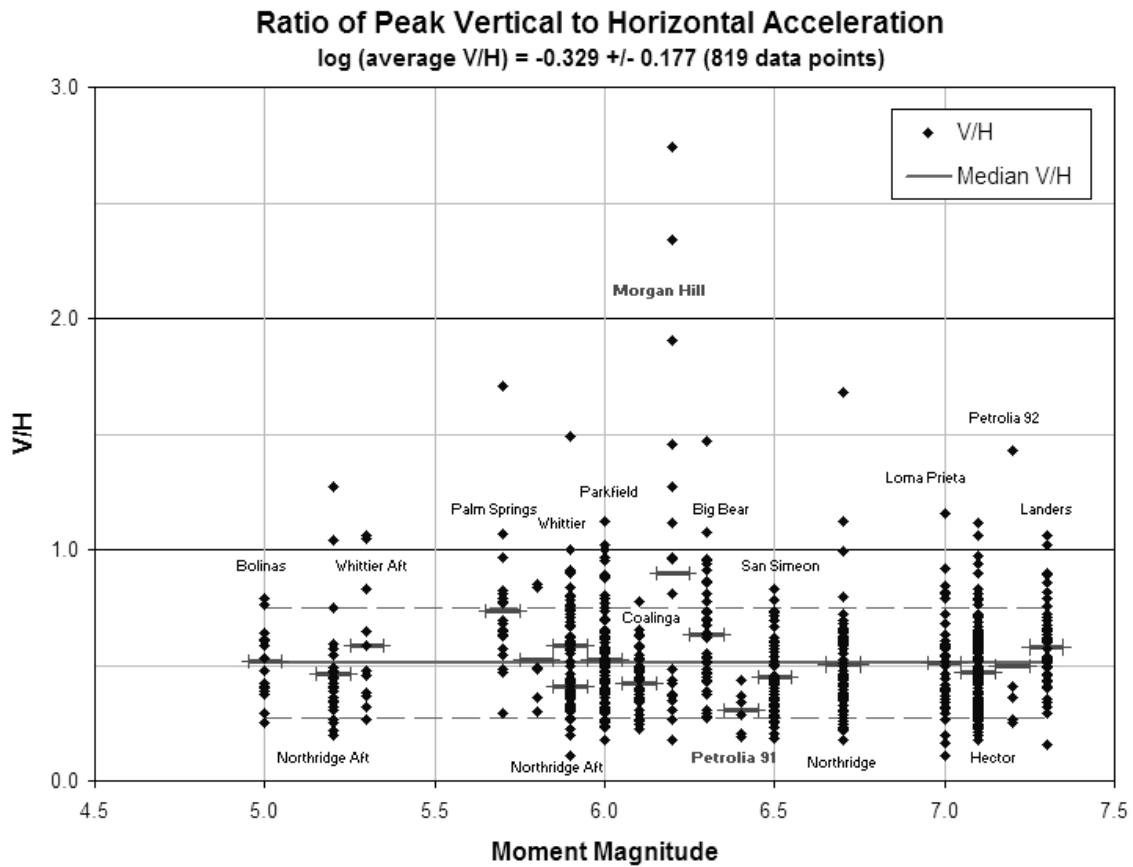


Fig. 1 Ratios of peak vertical to horizontal acceleration (V/H) from 18 Californian earthquakes (dashed lines indicate median +/- standard deviation and “++” marks median V/H ratio for each specific event)

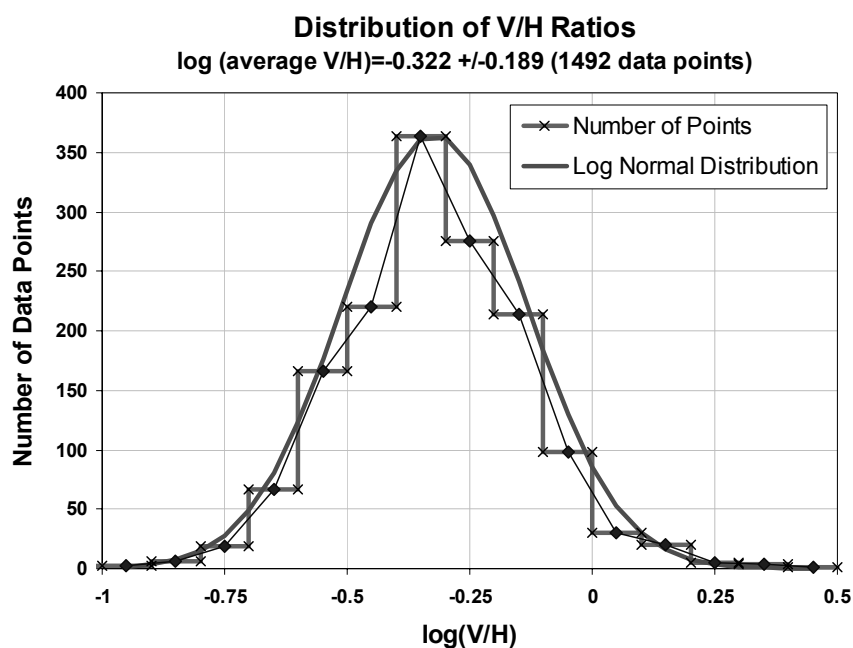


Fig. 2 Log-normal fit to V/H ratio

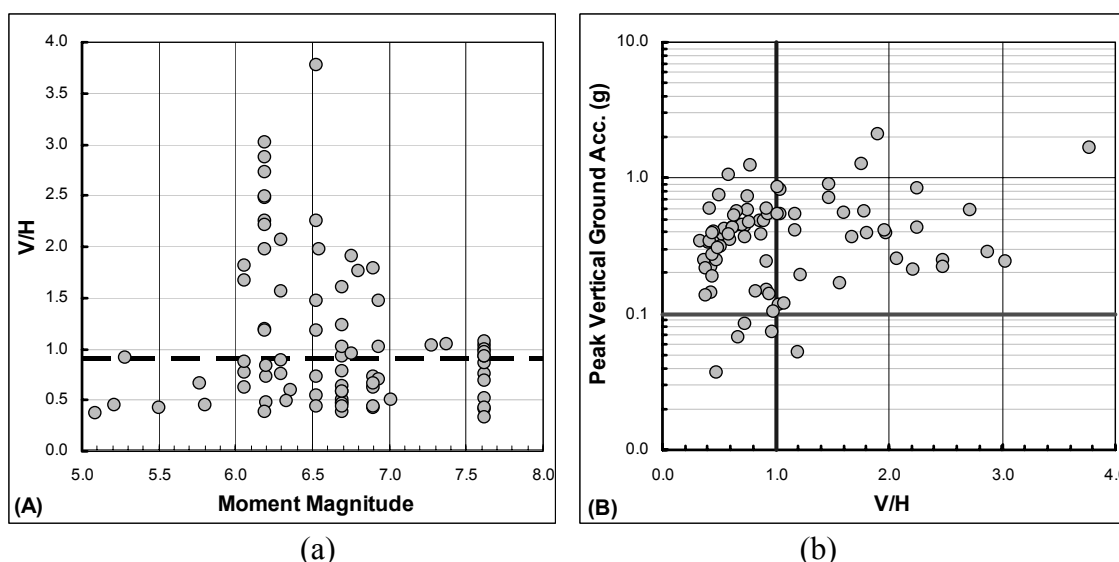


Fig. 3 Ratios of peak vertical to horizontal acceleration (V/H) plotted against (a) moment magnitude, and (b) peak vertical acceleration (dashed lines indicate the sample median)

Figure 3(a) shows the plot of the V/H ratio against the magnitude of the events. It may be seen that the median V/H ratio is equal to 0.9, being much higher than the commonly accepted value of 0.67 or the median of the mixed dataset (i.e., 0.47). The maximum V/H ratio in the subset is close to 4.0. This data point corresponds to the 1979 Imperial Valley earthquake ($M_w = 6.5$) and to the El Centro Array # 6 station, which recorded peak vertical ground acceleration of more than 1.6g. As mentioned earlier, the maximum vertical acceleration exceeding 2g was recorded during the Nahanni earthquake of 1985. This motion produced the vertical-to-horizontal peak ground acceleration ratio (V/H) of at least 2.0. The near-fault dataset used here implies that higher vertical acceleration tends to create larger V/H ratio as shown in Figure 3(b). Similar correlation, however, does not exist between the V/H ratio and peak horizontal acceleration.

The same trends that appeared in Figure 3 were not observed for the 2004 Parkfield event of magnitude 6.0. This relatively large strong-motion dataset (of 94 records) was studied separately by splitting it into two parts: near-fault data (41 data points recorded at distances less than 10 km from the fault) and other data (at more than 10 km from the fault). Interestingly, variations of V/H ratios with distance were found to be insignificant with the median of 0.49 being close to the median of the complete dataset (of 1400 records). The exercises conducted on different ground motion databases collectively confirm that V/H ratio may show significant variations, which depend on source and site characteristics and on seismic radiation pattern. Though not all earthquakes and their corresponding data from the near-fault region substantiate that V/H ratio is larger than unity, many data points confirm the opposite; hence influences of vertical component should not be ignored when seismic demands on structural components are assessed.

2. Rotational Component

Rotational components of ground motion (i.e., rocking and torsion) that are caused due to the incidence of SV-waves and surface waves have long been assumed to have low intensity compared to their horizontal and vertical counterparts; thus their impact on structural response is often overlooked. However, many structural failures and damage caused by the earthquakes can be linked not only to the translational but also to the rotational ground motions. For instance, torsional response of tall buildings in Los Angeles during the 1971 San Fernando, California earthquake could be attributed to the torsional excitation (Hart et al., 1975), while rotational and longitudinal differential motions may have caused the collapse of bridges during the San Fernando 1971 and Miyagi-ken-Oki 1978 earthquakes (Bycroft, 1980), and during the Northridge 1994 earthquake (Trifunac et al., 1996). Earthquake damage to pipelines, which is not associated with faulting or landslides and is due to large differential motions and strains in the soil, reflects the consequences of the propagating seismic waves and of the associated large rotations and twisting of soil blocks that are caused by lateral spreads and early stages of liquefaction (Ariman and Muleski, 1981; Trifunac and Todorovska, 1998).

Table 1: Near-Fault Ground Motion Subset

No.	Year	Event	Mw	Station Name	Peak Ground Acceleration (g)			V/H	Distance* (km)	VS30** (m/s)
					Hor.1	Hor.2	Ver.			
1	1987	Baja California	5.5	Cerro Prieto	1.39	0.89	0.59	0.42	-	660
2	1992	Cape Mendocino	7.0	Cape Mendocino	1.50	1.04	0.75	0.50	7.0	514
4	1999	Chi-Chi, Taiwan	7.6	CHY028	0.65	0.82	0.34	0.41	3.1	543
5	1999	Chi-Chi, Taiwan	7.6	CHY080	0.97	0.97	0.72	0.75	2.7	553
7	1999	Chi-Chi, Taiwan	7.6	TCU068	0.57	0.46	0.49	0.86	0.3	487
8	1999	Chi-Chi, Taiwan	7.6	TCU071	0.57	0.65	0.45	0.69	5.3	625
9	1999	Chi-Chi, Taiwan	7.6	TCU079	0.74	0.39	0.39	0.52	11.0	364
11	1999	Chi-Chi, Taiwan	7.6	TCU088	0.51	0.52	0.22	0.43	18.2	553
12	1999	Chi-Chi, Taiwan	7.6	TCU129	1.01	0.63	0.34	0.34	1.8	664
15	1999	Chi-Chi, Taiwan-06	6.3	TCU079	0.77	0.62	0.58	0.75	10.1	364
16	1999	Chi-Chi, Taiwan-06	6.3	TCU080	0.47	0.54	0.48	0.89	10.2	375
17	1983	Coalinga-02	5.1	Anticline Ridge Free-Field	0.58	0.67	0.25	0.37	-	376
18	1983	Coalinga-05	5.8	Oil City	0.87	0.45	0.57	0.66	-	376
19	1983	Coalinga-07	5.2	Coalinga-14th & Elm (Old CHP)	0.43	0.73	0.33	0.45	-	339
20	1983	Coalinga-01	6.4	Pleasant Valley P.P. - yard	0.59	0.55	0.35	0.60	8.4	257
21	1992	Erzincan, Turkey	6.7	Erzincan	0.50	0.52	0.25	0.48	4.4	275
22	1995	Kobe, Japan	6.9	KJMA	0.82	0.60	0.34	0.42	1.0	312
23	1995	Kobe, Japan	6.9	Takatori	0.61	0.62	0.27	0.44	1.5	256
24	1976	Gazli, USSR	6.8	Karakyr	0.61	0.72	1.26	1.76	5.5	660
25	1979	Imperial Valley-06	6.5	Bonds Corner	0.59	0.77	0.42	0.55	2.7	223
26	1979	Imperial Valley-06	6.5	El Centro Array #8	0.60	0.45	0.44	0.73	3.9	206
27	1995	Kobe, Japan	6.9	Nishi-Akashi	0.51	0.50	0.37	0.73	7.1	609
28	1995	Kobe, Japan	6.9	Takarazuka	0.69	0.69	0.43	0.62	0.3	312
29	1992	Landers	7.3	Lucerne	0.73	0.79	0.82	1.04	2.2	685
30	1989	Loma Prieta	6.9	Corralitos	0.64	0.48	0.46	0.71	3.9	462
31	1989	Loma Prieta	6.9	LGPC	0.56	0.61	0.89	1.47	3.9	478
33	1990	Manjil, Iran	7.4	Abbar	0.51	0.50	0.54	1.05	12.6	724
35	1986	N. Palm Springs	6.1	North Palm Springs	0.59	0.69	0.43	0.63	4.0	345
36	1986	N. Palm Springs	6.1	Whitewater Trout Farm	0.49	0.61	0.47	0.77	6.0	345
37	1985	Nahanni, Canada	6.8	Site 1	0.98	1.10	2.09	1.90	9.6	660
38	1994	Northridge-01	6.7	Beverly Hills - 12520 Mulhol	0.62	0.44	0.31	0.51	18.4	546
39	1994	Northridge-01	6.7	Castaic - Old Ridge Route	0.57	0.51	0.22	0.38	20.7	450
40	1994	Northridge-01	6.7	Newhall - Fire Sta	0.58	0.59	0.55	0.93	5.9	269
41	1994	Northridge-01	6.7	Pacoima Dam (upper left)	1.58	1.29	1.23	0.78	7.0	2016
42	1994	Northridge-01	6.7	Pardee - SCE	0.66	0.41	0.38	0.58	7.5	345
43	1994	Northridge-01	6.7	Rinaldi Receiving Sta	0.84	0.47	0.85	1.02	6.5	282
45	1994	Northridge-01	6.7	Simi Valley - Katherine Rd	0.88	0.64	0.40	0.46	13.4	557
46	1994	Northridge-01	6.7	Sylmar - Olive View Med FF	0.60	0.84	0.54	0.63	5.3	441
47	1994	Northridge-01	6.7	Tarzana - Cedar Hill A	1.78	0.99	1.05	0.59	15.6	257
48	1994	Northridge-06	5.3	Rinaldi Receiving Sta	0.65	0.43	0.60	0.92	-	282
49	1986	San Salvador	5.8	Geotech Investig Center	0.87	0.48	0.39	0.45	6.3	545
50	1980	Victoria, Mexico	6.3	Cerro Prieto	0.62	0.59	0.30	0.49	14.4	660
51	1999	Chi-Chi, Taiwan	7.6	TCU103	0.13	0.16	0.15	0.92	6.1	494
52	1999	Chi-Chi, Taiwan	7.6	TCU118	0.11	0.09	0.12	1.03	26.8	215
53	1999	Chi-Chi, Taiwan	7.6	CHY092	0.08	0.11	0.12	1.07	22.7	254
54	1999	Chi-Chi, Taiwan	7.6	TCU141	0.08	0.11	0.10	0.99	24.2	215
55	1999	Chi-Chi, Taiwan	7.6	CHY026	0.08	0.07	0.07	0.97	29.5	226
56	1999	Chi-Chi, Taiwan	7.6	TCU122	0.22	0.26	0.24	0.92	9.4	475
58	1999	Chi-Chi, Taiwan-03	6.2	TCU116	0.12	0.11	0.08	0.73	22.1	493
59	1999	Chi-Chi, Taiwan-06	6.3	TCU075	0.06	0.11	0.17	1.56	26.3	573
60	1999	Chi-Chi, Taiwan-06	6.3	TCU076	0.11	0.12	0.26	2.07	25.9	615
61	1979	Imperial Valley-06	6.5	El Centro Array #6	0.41	0.44	1.66	3.77	1.4	203
62	1979	Imperial Valley-06	6.5	Agrarias	0.37	0.22	0.83	2.25	0.7	275
63	1979	Imperial Valley-06	6.5	El Centro Array #7	0.34	0.46	0.54	1.18	0.6	211
64	1979	Imperial Valley-06	6.5	El Centro Differential Array	0.35	0.48	0.71	1.47	5.1	202
65	1980	Irpina, Italy-01	6.9	Bisaccia	0.10	0.08	0.07	0.67	21.3	1000
66	1980	Irpina, Italy-02	6.2	Calitri	0.18	0.16	0.15	0.83	8.8	600
67	1995	Kobe, Japan	6.9	Port Island (0 m)	0.31	0.28	0.56	1.79	3.3	198
68	1989	Loma Prieta	6.9	Capitola	0.53	0.44	0.54	1.02	15.2	289
69	1980	Mammoth Lakes-01	6.1	Convict Creek	0.42	0.44	0.39	0.88	6.6	339
70	1984	Morgan Hill	6.2	Gilroy Array #2	0.16	0.21	0.58	2.72	13.7	271
71	1984	Morgan Hill	6.2	Hollister Diff Array #4	0.10	0.09	0.28	2.87	26.4	216
72	1984	Morgan Hill	6.2	Hollister Diff Array #5	0.10	0.10	0.25	2.47	26.4	216
73	1984	Morgan Hill	6.2	Hollister Diff Array #3	0.08	0.08	0.24	3.02	26.4	216
74	1984	Morgan Hill	6.2	Gilroy Array #7	0.19	0.11	0.43	2.25	12.1	334
75	1984	Morgan Hill	6.2	Hollister Diff. Array	0.09	0.09	0.22	2.48	26.4	216
76	1984	Morgan Hill	6.2	Hollister Diff Array #1	0.10	0.09	0.21	2.22	26.4	216
77	1984	Morgan Hill	6.2	Gilroy Array #3	0.19	0.20	0.40	1.97	13.0	350
78	1984	Morgan Hill	6.2	San Juan Bautista, 24 Polk St	0.04	0.04	0.05	1.19	27.2	371
79	1984	Morgan Hill	6.2	Gilroy Array #4	0.22	0.35	0.41	1.17	11.5	222
80	1986	N. Palm Springs	6.1	Morongo Valley	0.22	0.20	0.40	1.81	12.1	345
81	1986	N. Palm Springs	6.1	Cabazon	0.22	0.21	0.36	1.67	7.8	345
82	1985	Nahanni, Canada	6.8	Site 3	0.15	0.14	0.14	0.95	5.3	660
83	1994	Northridge-01	6.7	Arieta - Nordhoff Fire Sta	0.34	0.31	0.55	1.61	8.7	298
84	1994	Northridge-01	6.7	Sunland - Mt Gleason Ave	0.13	0.16	0.19	1.23	13.4	446
85	1987	Superstition Hills-02	6.5	Wildlife Liquef. Array	0.18	0.21	0.41	1.97	23.9	207
91	1979	Imperial Valley-06	6.5	Aeropuerto Mexicali	0.33	0.26	0.14	0.44	0.3	275
94	1980	Irpina, Italy-02	6.2	Sturno	0.07	0.08	0.04	0.47	20.4	1000
97	1994	Northridge-01	6.7	Pacoima Dam (downstr)	0.42	0.43	0.19	0.44	7.0	2016
98	1966	Parkfield	6.2	Temblor pre-1969	0.36	0.27	0.14	0.38	16.0	528

* Closest distance to fault; ** Average shear-wave velocity for the first 30m

Most instruments used in the seismological practice to record ground motions are pendulum seismographs, velocigraphs or accelerographs. Such instruments are accurately sensitive to the translational motion of their base provided that there is no tilting. Translational components during a seismic event are however accompanied by rotational components because of the traveling wave effects. Studies have showed that tilting of the recorder's base can severely contaminate its response; thereby, the recorded data may become the mixture of translational and rotational motions, and may be far from representing the true acceleration, velocity and displacement in the direction of recording. A number of attempts to measure rotational motion resulted in measurements from explosions, but not from earthquakes (e.g., Kharin and Simonov, 1969; Graizer, 1989; Nigbor, 1994). In the absence of having records of rotational motion, the attempts have been made to define them in terms of the recorded translational components (Trifunac and Hudson, 1971; Lee and Trifunac, 1985; Niazi, 1986; Lee and Trifunac, 1987; Graizer, 1987, 1989, 1991; Oliveira and Bolt, 1989; Takeo and Ito, 1997; Huang, 2003). An effective method of tilt evaluation using uncorrected strong-motion accelerograms was first suggested by Graizer (1989). It was later tested in a number of laboratory experiments at the USGS, Menlo Park, with different strong-motion instruments. Graizer's method is based on the difference in the tilt sensitivity of the horizontal and vertical pendulums. This method was successfully applied to a number of strong ground motion records of the 1994 Northridge earthquake ($M_w = 6.7$) to extract the rotational motions. Among many records from the stations that recorded the Northridge earthquake, a dramatic case was observed at the Pacoima dam—upper left abutment where the residual tilt reached 3.1° in the $N45^\circ E$ direction. It was a result of local earthquake-induced tilting due to the high-amplitude ground shaking (Graizer, 2006a; Kalkan and Graizer, 2007). The computed value of residual tilt was in good agreement with the tilt measured using electronic level a few days after the earthquake (Shakal et al., 1994). Figure 4 depicts the 210° -component horizontal and vertical motions recorded at the Pacoima dam along with the computed rotational component for a cross-comparison. Details of extracting rotational component for this specific station can be found in Graizer (2006a).

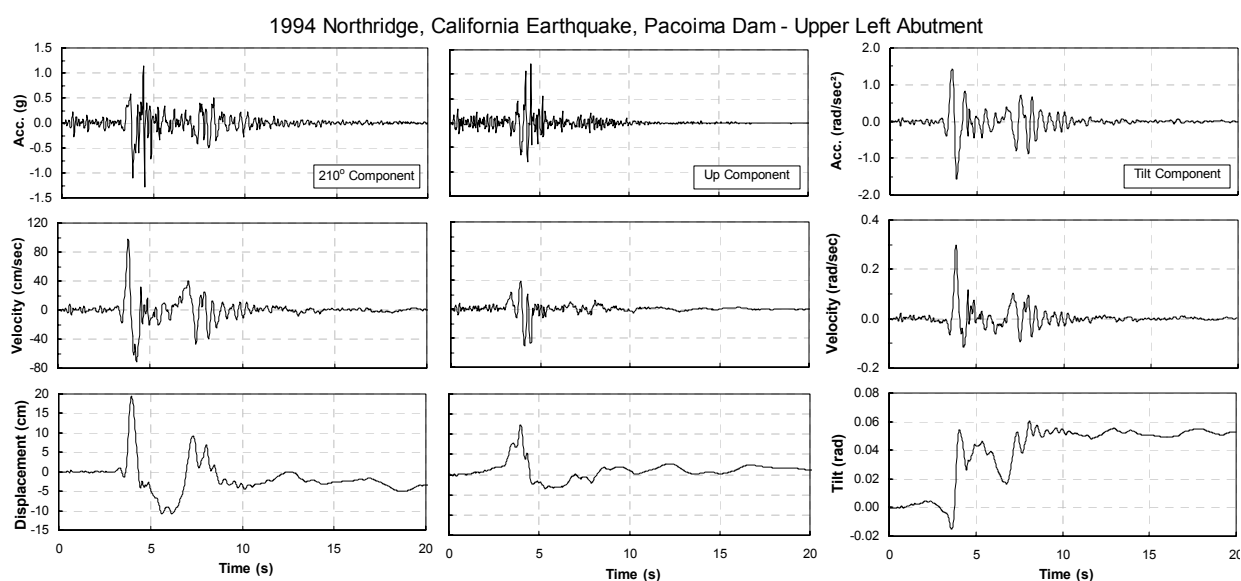


Fig. 4 Horizontal, vertical and tilt components of the Pacoima dam upper left abutment record during the 1994 Northridge earthquake (panels show only the first 20 s of motions)

The tilt motion function obtained from the acceleration record demonstrates the tilt rising from zero to the level of about 3.1° in a period of 3.5 to 8.0 s from the beginning of recording. The main tilt increase (which is a step-type function) is found to correlate well with the highest level of recorded acceleration that occurred with the arrival of strong phase of the S-wave. The estimated velocity of tilting results in a maximum amplitude of about 15° per second (0.26 rad/sec). The residual tilt of about 3.1° (0.054 rad) produces the same result in the accelerometer response as an acceleration of about 0.05g. The two components of translational motion and tilt at Pacoima dam, as shown in Figure 4, are used as the input data (without scaling) for the transient analyses, results of which are presented in the later sections.

UNCOUPLED AND COUPLED GOVERNING EQUATIONS OF MOTION

In the following, uncoupled response of a SDOF oscillator is first revisited to establish a theoretical basis for the derivation of governing equation of motion of a SDOF oscillator when it is subjected to translational, vertical and/or tilting excitations in tandem. It should be noted that all equations derived and the results, which follow, are valid provided that relative displacement of oscillator satisfies the condition, $\sin \phi \cong \phi$, where ϕ is the chord rotation.

1. Uniaxial Translational Excitation

Dynamic equilibrium of the mass m of the inverted pendulum (i.e., a SDOF oscillator) with stiffness k and damping c shown in Figure 5(a) yields

$$m\ddot{u} + c\dot{u} + ku = -m\ddot{u}_g \quad (1)$$

where u is the relative displacement of the oscillator with respect to the ground, and \ddot{u}_g is the ground-induced translational acceleration. For the sake of simplicity, the SDOF oscillator is represented by a rigid bar, and system flexibility is lumped in a rotational spring at the base. The initial stiffness of the system is denoted as k_0 , and a stable bilinear material model with the post-yield stiffness ratio of κ is assumed. The resistance force V is a function of the relative displacement u . The force-deformation plot shown in Figure 5(a) indicates the response of a SDOF oscillator to the translational motion only, whereby the destabilizing effect of the axial load (i.e., P- Δ effect) in the deformed position is ignored. As shown, u can be computed as ϕl for small angles ($\sin \phi \cong \phi$). The P- Δ effects on the response is considered next in Figure 5(b) in which the secondary moment, created by the axial load times the relative displacement u , is represented by the equivalent force-couple $mg\phi$ acting on the mass of the system. Since ϕ is a function of the response parameter u , it is convenient for numerical computations to cast this additional forcing function in a geometric-stiffness term, k_G ($= mg/l$), on the left side of Equation (1). The ratio of the geometric-stiffness term to the initial stiffness yields the well-known stability coefficient, θ :

$$\theta = k_G / k_0 \quad (2)$$

The stiffness apparent in the second-order analysis is called as “effective stiffness”. In the pre-yield condition, it is equal to $k = k_0(1 - \theta)$, while in the post-yield condition it can be expressed as $k = k_0(k - \theta)$. Thus, effective period of the structure, T , accounting for the P- Δ effects, is expressed as

$$T = T_0 / \sqrt{1 - \theta} \quad (3)$$

where T_0 is based on the initial stiffness of the first-order analysis. The dynamic equilibrium equation nesting P- Δ effects in the geometric-stiffness term can be expressed as

$$m\ddot{u} + c\dot{u} + (k_0 - k_G)u = -m\ddot{u}_g \quad (4)$$

For nonlinear response, Equation (4) can be solved incrementally in the time domain by replacing k_0 by instantaneous tangent stiffness that varies according to the hysteretic behavior of the system. Unlike tangent stiffness, the geometric-stiffness term remains unchanged in the inelastic range (provided that there is no vertical excitation). It is also instructive to note that initial period and effective stiffness change by including the P- Δ effects. On the other hand, yield displacement (u_y) remains unchanged, since u_y is directly related to the moment-curvature behavior at the section level, while the P- Δ phenomenon becomes effective at the global system level.

2. Coupled Translational and Tilt Excitations

To fully understand the response of a SDOF oscillator to the tilt motion, it is convenient to examine the P- Δ effects separately. First let us think of a SDOF oscillator with a concentrated mass and height (l) as illustrated in Figure 6(a). When it is subjected to base rotation only, the oscillator mass is influenced by the inertial force (F_α) due to the angular acceleration ($\ddot{\alpha}$). This inertia force is expressed as

$$F_\alpha = m\ddot{\alpha}l \tag{5}$$

It is possible to represent the rotating-base oscillator in Figure 6(a) by an equivalent fixed-base oscillator as illustrated in Figure 6(b). This representation has some computational advantages, especially for the inelastic systems. It directly provides the relative drift associated with the exact deformation. The response of an equivalent fixed-base oscillator therefore does not include the rigid body rotation (α), yet it includes the forcing effects of this rotation. It means that the relative rotations (ϕ) of the rotating-base and fixed-base oscillators become identical, while the total rotation of the fixed-base oscillator can be obtained explicitly by summing up α (i.e., base tilting) and ϕ .

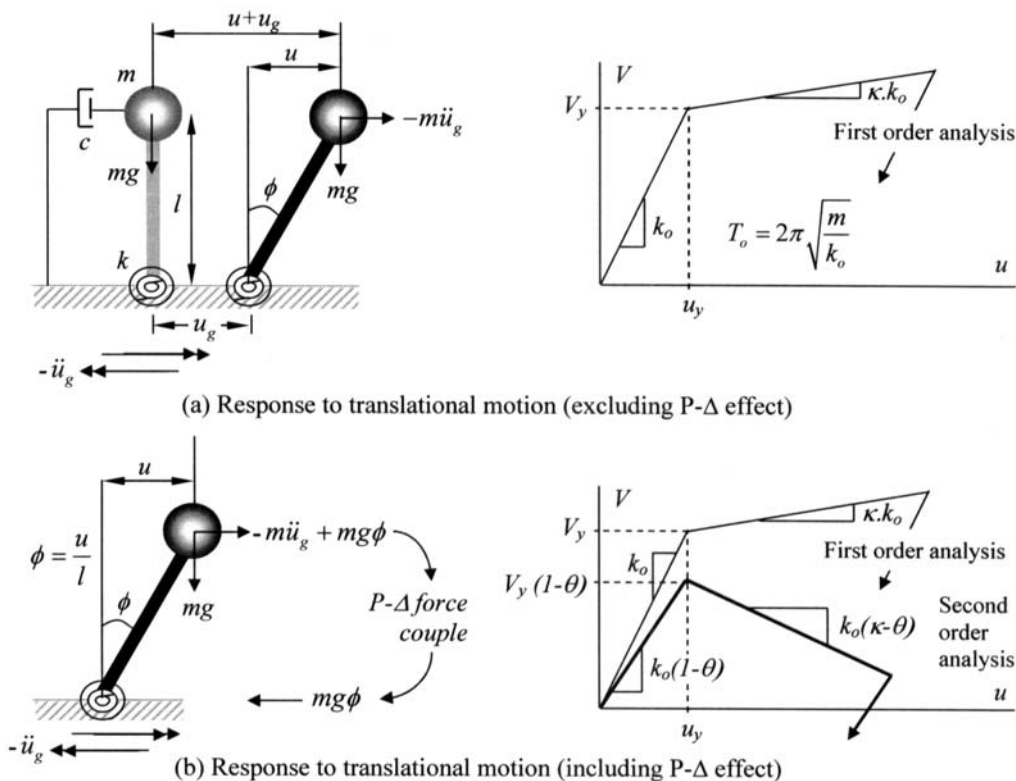


Fig. 5 Fixed-base SDOF oscillator subjected to translational ground motion

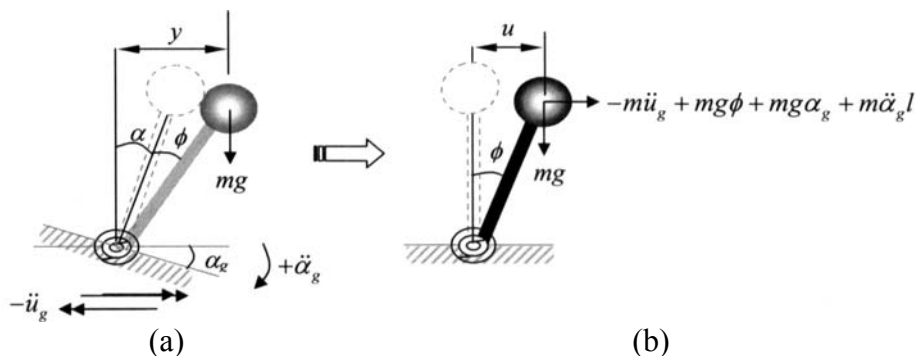


Fig. 6 (a) SDOF oscillator subjected to the coupled tilt and translational ground motion; (b) Equivalent fixed-base system

When the rotating-base oscillator is subjected to the coupled tilt and translational components of ground motion, the resultant force on the corresponding equivalent fixed-base oscillator can be represented by superposing the two inertia forces caused by the translational and angular accelerations (i.e., $-m\ddot{u}_g + m\ddot{\alpha}l$). As evident in Figure 6(a), the additional rigid-body rotation due to the base tilting amplifies the P-Δ effects by increasing the moment arm. In this case, it is convenient to decompose the

total P- Δ contribution into two components. The first component originates due to the base tilting (α) and can be represented as an additional forcing function since it is independent of the oscillator response. The second P- Δ component is a direct consequence of the relative oscillator response (ϕ), and therefore, it can be treated within the geometric-stiffness term (k_G). Again, the total rotation of a fixed-base oscillator can be obtained by adding the base rotation (α) to the system relative rotation (ϕ). Figure 6(b) illustrates the complete forcing function acting on the mass of the equivalent fixed-base oscillator when it is subjected to the coupled tilt and translational motion. The corresponding dynamic equilibrium equation of this physical system can be written as

$$m\ddot{u} + c\dot{u} + ku = -m\ddot{u}_g + mg\phi + mg\alpha_g + m\ddot{\alpha}_g l \quad (6)$$

Equation (6) can also be derived using the Lagrange formulation based on equilibrium of potential and kinetic energies. By representing the P- Δ component due to ϕ as $k_G u$, Equation (6) can be alternatively expressed in the following form:

$$m\ddot{u} + c\dot{u} + (k_0 - k_G)u = -m\ddot{u}_g + mg\alpha_g + m\ddot{\alpha}_g l \quad (7)$$

Equation (7) is theoretically complete to solve the translational response of a SDOF oscillator when it is concurrently subjected to translational and tilting excitations. In the derivation of Equations (6) and (7), positive angular acceleration and corresponding ground tilting are assumed to be in the clockwise direction.

3. Coupled Horizontal, Vertical, Angular Accelerations, and Tilt

In the preceding sections, the effects of vertical ground motion on the translational response of an oscillator are ignored, and the geometric stiffness term of a unit mass system, being a function of the gravitational acceleration and the length of an oscillator, is defined as $k_G = g/l$. In such a case, k_G denotes the characteristics of the SDOF system only: it retains a constant value throughout the elastic or inelastic oscillations while being unaffected by the input motion. Conversely, coupling of vertical excitation with the translational component of motion carries the geometric-stiffness term from static to the dynamic state. Thus, instead of having a constant value, geometric-stiffness term becomes a function of vertical acceleration, and takes the following form:

$$k_G' = \frac{g - \ddot{z}_g}{l} \quad (8)$$

Equation (8) is derived considering a unit-mass system, and upward direction in vertical accelerograms is assumed to be positive. The following discussion is also based on these conditions. Recall that tilt excitation has no influence on geometric stiffness, yet it creates additional P- Δ forces as demonstrated in Figure 6(b). On the other hand, geometric-stiffness term given in Equation (8) becomes time-dependent, and such dynamism creates several complications. As such, k_G' fluctuates, during the transient analysis, around the static geometric-stiffness term (g/l), while its deviation from k_G depends on the relative amplitude of the vertical excitation (\ddot{z}_g) with respect to the gravitational constant. It may show significant differences from its static constant value, which is less than k_G , if the peaks of vertical component are in the upward direction and their amplitudes are closer to or larger than the gravitational acceleration. As a consequence of this, the overall stiffness of an elastic SDOF oscillator (i.e., $k_0 - k_G'$) becomes time-variant. It is, therefore, not possible to have a constant-period oscillator in the elastic domain when the effects of vertical excitation are included. Coupling of high-intensity vertical excitation with the translational motion may initiate a nonlinear elastic system where the oscillation period varies in time, and returns to its initial value at the termination of the ground motion.

Another important complication associated with considering the vertical motion is the eroded overall stiffness of the oscillator due to possible adverse impacts from the geometric-stiffness term. Such effects are even more severe for the inelastic systems where the vertical component may constantly change not only the pre-yield but also the post-yield force-deformation slope (it creates wave-effect on the hysteretic loops as will be shown later). If the vertical component of motion has enough intensity and its peaks are in-phase with the gravity (i.e., it is downward), the associated value of enhanced geometric-stiffness term

leads to ratcheting of the displacement response, which may eventually ensue dynamic instability in the system. It is also noteworthy that the geometric-stiffness term yields larger values as the length of the oscillator decreases. Under the coupled vertical and translational motion, the equation of motion of a SDOF oscillator yields the following form:

$$m\ddot{u} + c\dot{u} + (k_0 - k'_G)u = -m\ddot{u}_g \tag{9}$$

Equation (9) is complete for the SDOF oscillator response in translational direction considering the coupling of vertical excitation only. Incorporating the tilting component does not create any change on the left side of Equation (9); it introduces additional forcing functions on the right side of the equation, as in the case of coupling of horizontal and tilting excitations (see Equation (7)). The first additional forcing term is the inertial force ($= m\ddot{\alpha}_g l$) due to the angular acceleration. Its amplitude escalates as the length of the oscillator increases. The second forcing term ($= m(g - \ddot{z}_g)\alpha$) is a supplemental P-Δ force pair due to the coupling of tilting and vertical components. The inclusion of these two forcing functions in Equation (9) yields the theoretically inclusive governing equation of motion for a SDOF oscillator under the influence of multi-component excitations, including horizontal, vertical, and angular accelerations, and ground tilting. This equation is expressed as follows:

$$m\ddot{u} + c\dot{u} + (k_0 - k'_G)u = -m\ddot{u}_g + m(g - \ddot{z}_g)\alpha_g + m\ddot{\alpha}_g l \tag{10}$$

Equation (10) is derived for the SDOF oscillator illustrated in Figure 7(a) where three components of ground shaking are acting on the base of the oscillator. The corresponding forcing functions acting on the mass of the equivalent fixed-base oscillator are illustrated in Figure 7(b). It is worth mentioning that depending on the sign-convention for the angular, vertical and translational accelerations, signs of the forcing functions in Equations (6) and (10) may change (see Figures 6 and 7 for the compatible sign-convention used in the derivation of these equations). As mentioned earlier, the equivalent fixed-base model is easy to implement in a computational framework, particularly for the inelastic systems, since it directly provides the relative drift associated with the exact deformation in the horizontal plane. Once again, the response of an equivalent fixed-base oscillator does not include the rigid body rotation (α), yet it includes the forcing effects of this rotation. It means that the relative rotations (ϕ) of the rotating-base and fixed-base oscillators become identical while the total rotation of the fixed-base oscillator can be obtained explicitly by summing α (i.e., base tilting) and ϕ .

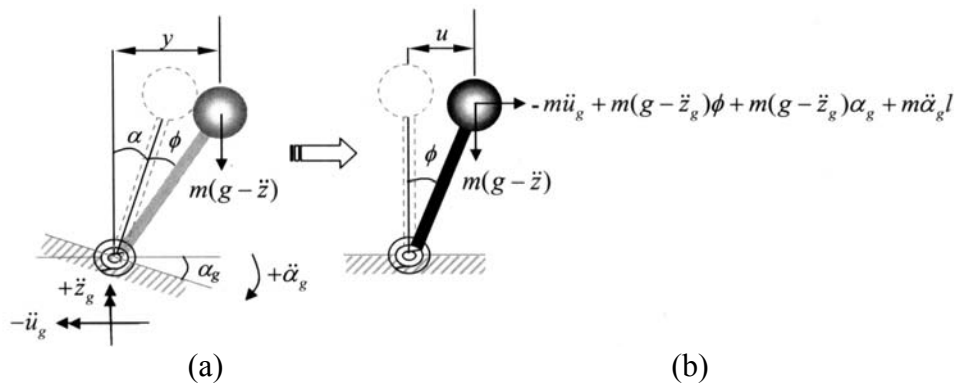


Fig. 7 (a) SDOF oscillator subjected to the coupled tilt, translational and vertical components of ground motion; (b) Equivalent fixed-base system

Based on a new geometric-stiffness formulation given in Equation (8), the stability coefficient can be rewritten as $\theta' = k'_G / k_0$, where θ' now is a function of the vertical excitation. It is obvious that θ' should remain less than unity to maintain stability. Figure 8 compares the plots of the force-deformation relation for the first- and second-order analyses of a SDOF oscillator. Notably, effective yield force ($= V_y (1 - \theta')$) also becomes time-variant while the yield displacement (u_y) remains unchanged.

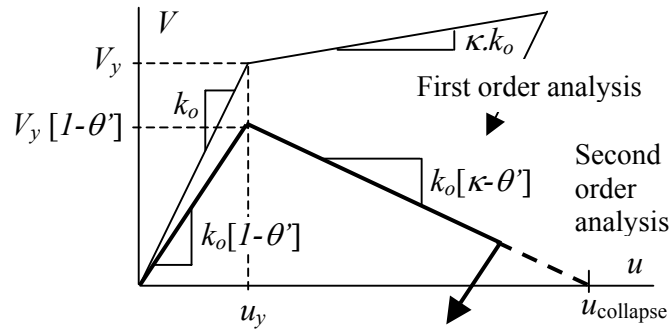


Fig. 8 Force-deformation relation under the coupled tilt, translational and vertical components of ground motion (in second-order analysis, for both pre-yield and post-yield slopes, $V-u$ diagram is conditionally drawn as straight line; in reality, the vertical component may progressively change the slope and create a wave-effect)

It may be noted that θ varies with a change in system stiffness, as implied by Equation (2), meaning that it is a function of the spectral period. Therefore, θ cannot serve as a convenient parameter for direct use in a spectral format unless l (i.e., height or length of the oscillator) is varied at each spectral period to keep θ constant. In lieu of θ , Kalkan and Graizer (2007) proposed a new descriptor, called “geometric oscillation period”, for use as a spectral-period-independent P- Δ parameter. It was originally developed from the P- Δ force pair (i.e., $F_{P-\Delta} = (mg/l)u = k_G u$) for a unit-mass system by neglecting the vertical excitation effects, and it is expressed as

$$T_G = 2\pi\sqrt{l/g} \tag{11}$$

It may be recalled that vertical excitation transforms T_G into a dynamic form:

$$T'_G = 2\pi\sqrt{l/(g-\ddot{z}_g)} \tag{12}$$

T'_G is still independent of the oscillator stiffness but it becomes a function of the vertical excitation; therefore, it is not an invariant parameter, whereas T_G is. It is important to realize that, if the value of $(g-\ddot{z}_g)$ becomes zero (i.e., if $\ddot{z}_g(t) = g$ at a certain time-instant, t), the geometric-stiffness term becomes zero and P- Δ effects are instantaneously deactivated. In parallel, if $(g-\ddot{z}_g)$ yields negative sign, P- Δ effects tend to stabilize the system by changing the direction of P- Δ force towards the opposite direction of inertia force (in the loading cycle). If the system is in the unloading cycle, it can be in the same direction as the inertia force. Vertical excitation is a dynamic parameter, and depending on its intensity in time, it may help to stabilize the system by acting against gravity or destabilize the system by being in phase with the gravity. In parallel, T_G is aimed to serve as a controlling parameter for instability similar to θ . It is independent of the system period (i.e., stiffness), yet it is a function of the vertical acceleration. In this respect, T'_G can be either real-valued, infinite (if $\ddot{z}_g(t) = g$), or complex-valued. Complex value of T'_G implies that the P- Δ force is in the stabilizing mode; on the other hand, its real value indicates that the P- Δ force is in the destabilizing mode. From the structural design and performance assessment point of view, real value of T'_G is a meaningful parameter since it reflects the combined adverse impact of gravity and vertical excitation towards destabilizing the system. For this reason, the following formulations (Equations (13) and (14)) are conditioned on the real-valued T'_G .

The squared ratio of the elastic vibration period (T_0) to the geometric oscillation period (T'_G) defines the time-variant stability coefficient alternatively as

$$\theta' = k'_G/k_0 = (T_0/T'_G)^2 \tag{13}$$

It is also possible to derive relation between the instantaneous pre-yield effective period ($T_{\text{eff}}(t)$) of the system and the geometric oscillation period (T_G') as

$$T_{\text{eff}}(t) = T_0 T_G' / \sqrt{T_G'^2 - T_0^2}; \quad t \leq t_{\text{yield}} \quad (14)$$

where t is the time-instant before yielding. Note that the pre-yield effective period is no longer a constant value due to the vertical excitation; it may change at every time-instant. More importantly, Equation (14) indicates that if the geometric oscillation period of the system (T_G') becomes equal to or smaller than the initial elastic period (T_0), the instability (i.e., $\theta' \geq 1.0$) in the system is initiated. For a stable system, geometric oscillation period should be greater than the initial elastic period. Therefore, T_G' can serve as a valuable tool in seismic design to prevent geometric instability by quantifying lower bound for the lateral stiffness, while considering possible effects of vertical shaking in advance (to be on the conservative side, peak intensity of the vertical motion should be assumed to be in phase with the gravity).

HYSTERETIC BEHAVIOR AND DYNAMIC INSTABILITY

More insight into the progression of dynamic collapse associated with the negative post-yield stiffness due to the presence of enhanced P- Δ effects is conceptually illustrated on a bilinear hysteretic behavior shown in Figure 9. For the sake of simplicity, this figure focuses on the first few (imaginary) inelastic cycles and ignores the vertical excitation effects on the geometric stiffness.

It is apparent that second-order analysis reduces the yield strength by $(1 - \theta)$; therefore, first yielding of the system takes place at point A instead of A' while the yield displacement (u_y) remains unchanged. Following the yielding, velocity of the oscillator becomes zero when the oscillator hits the point B . It means that the kinetic energy of the system becomes zero and the oscillator reaches its positive peak displacement within the first inelastic cycle. Upon unloading, the oscillator moves to the other direction (towards O_1) with increasing negative velocity. Maximum velocity of the system occurs when the inertia force equals zero (i.e., at the points O_1, O_2). Between O_1 and C , the oscillator slows down. If the ground motion pulse has enough energy to overcome the effective yield strength (if f_c reaches f_c'), the oscillator may advance to left (i.e., in the negative displacement direction) and create an additional plastic half-cycle. Note that the stored strain energy in the system is not sufficient to push the oscillator beyond the point C on the way to the yield line (C'); hence the oscillator does not yield again and comes to rest at the point C . With the incoming of additional pulses, it returns towards B' . Due to the initiation of negative post-yield stiffness, the effective yield strength in the positive displacement direction becomes smaller than that in the negative displacement direction. Therefore, in the next cycle if the incoming pulses are sufficiently strong, the system may tend to move towards right where the yield strength is much less than that for the opposite direction ($f_D < f_E$). In other words, much larger impulses would be needed to overcome the effective yield strength, for instance f_E , in order to cause the system to advance inelastically to the left. For that reason, intensity level of the pulses needed to yield the system in one direction becomes progressively smaller, and inelastic deformation accumulates inherently in one direction and advances the system towards dynamic instability. In this perspective, $(\kappa - \theta)$ becomes an important parameter controlling the cumulative unidirectional deformation.

As Figure 9 indicates, instability in the system occurs when the unidirectional deformation accumulation reaches u_{collapse} ; beyond that, the inertia force would be negative while the system would advance in the positive displacement direction due to the axial load (Jennings and Husid, 1968; Sun et al., 1973; Akiyama, 1985; Ishida and Morisako, 1985). Therefore, u_{collapse} is the limiting point at which collapse in the system gets initiated. The effect of negative post-yield stiffness on the system stability is, in fact, not restricted to the bilinear material model referenced; its severity depends on the unloading and reloading rules of the material model used.

Based on the geometry shown in Figure 9 and on using negative post-yield slope, it is possible to approximate the onset of dynamic collapse as

$$u_{collapse} = u_y \frac{\kappa - 1}{\kappa - \theta} \tag{15}$$

Vertical component effects on the P-Δ effects are not included in the derivation of Equation (15); therefore, approximation of the collapse displacement ($u_{collapse}$) requires knowledge only on the yield displacement (u_y), stability coefficient (θ), and on the post-yield stiffness ratio (κ). All of these parameters are known in advance; hence, collapse displacement and associated collapse ductility demand can be estimated via Equation (15) before commencing the transient analysis. It should be noted that Equation (15) can be effectively used to provide a limiting criteria for assessing the tendency for the dynamic collapse of elasto-plastic structural systems. Its formulation is still valid for a simple stiffness-degrading model; yet it may need to be reformulated when different material models are utilized. Inclusion of vertical motion effects in Equation (15) again requires its reformulation since θ now becomes a function of the vertical acceleration pulses (see Equation (13)).

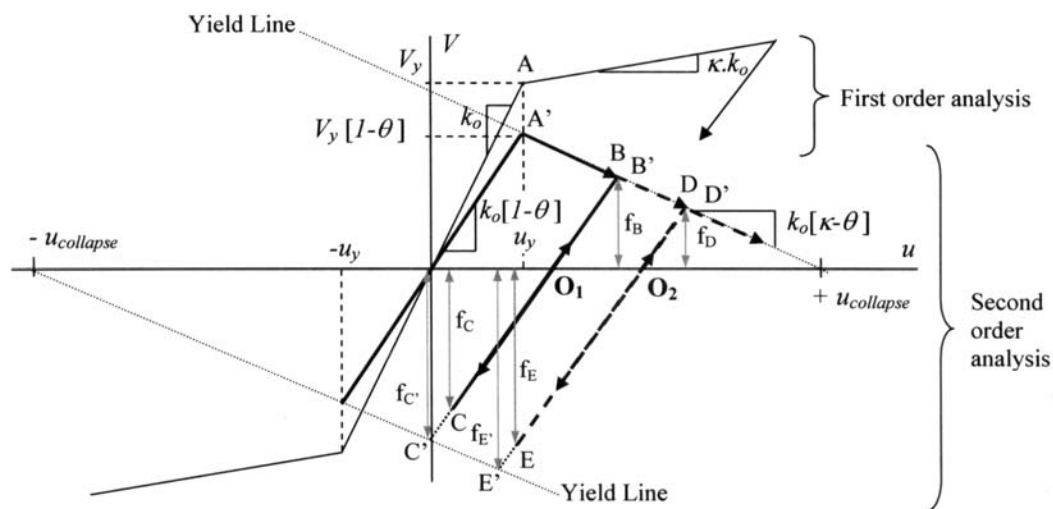


Fig. 9 Progression of dynamic collapse due to the P-Δ effects

RESULTS FROM INELASTIC SDOF ANALYSES

In the previous sections, a set of governing equations of motions for a SDOF oscillator is developed considering different combinations of input motion components. Based on this, an inelastic SDOF oscillator is next subjected to uncoupled and coupled combinations of the three components (i.e., horizontal, vertical and tilting). Results from the inelastic transient analyses are presented in a comparative way to distinguish the relative impacts produced by each component. It should be noted that the horizontal component is applied in each case, while its coupling combinations with the other components are systematically varied. Sign of the vertical motion is also changed to gauge the effects of phase difference.

In order to obtain a realistic set of results, a single-column bent of a highway viaduct (which is a part of a freeway) is used as the reference structure (see Figure 10(a)). This configuration of the bridge bent was previously utilized as a design model by Chopra and Goel (2001). The superstructure has a total weight of 190 kN/m, and is supported on identical bents uniformly spaced at 39.6 m. For the purpose of response evaluation in the transverse direction, the viaduct can be idealized as a SDOF oscillator (see Figure 10(c)). The properties of SDOF oscillator were carefully tuned so as to represent the design dynamic characteristics of the bridge bent in terms of mass, stiffness, damping, height and force-deformation relation. Some of the relevant design parameters are provided in Figure 10(b). Inelastic material behavior is characterized by the rate-independent elasto-plastic model of Ozdemir (1976) with 2 percent kinematic strain hardening (κ). The system under consideration was initially designed by Chopra and Goel (2001) for a ductility (u_d) of 3.25 while ensuring that the plastic rotation at the base of the

column was limited to 0.02 rad. Foundation flexibility and associated rocking response as well as P-Δ effects were not considered in the design process.

The idealized SDOF system shown in Figure 10(c) is taken as a proxy and is subjected to a series of nonlinear transient analyses. First, the translational component of Pacoima Dam record (see Figure 4) is set as an input without paying attention to the P-Δ effects (to be referred to as Case-1). Figure 11 portrays the inelastic results from Case-1 in which the peak relative displacement reaches 26.5 cm (~ 3 percent drift) and produces a ductility demand of 3.24. In the left panel of this figure, y-axis indicates the normalized base shear. Note that the displacement values ($u = \phi l$) plotted are relative values computed from the relative rotation of the oscillator's mass with respect to its base. The computed ductility demand is almost equal to the design ductility level ($\mu_d = 3.25$), implying that the horizontal component of the Pacoima Dam record satisfies the design requirement at a minimum level with no reservations; thereby it can serve as a benchmark against which relative impacts of multi-component excitations on seismic response can ideally be compared and contrasted. Figure 11 also shows the input force time-history normalized by mass, which is same as the ground acceleration (\ddot{u}_g) for this particular case. From the time-response plot, it is possible to observe that the overall deformation demand in the system is produced by a few plastic cycles initiated by the first major acceleration pulse arrival between 3 and 5 s and followed by the second acceleration pulse arrival between 7 and 8 s (see the two right panels in Figure 11).

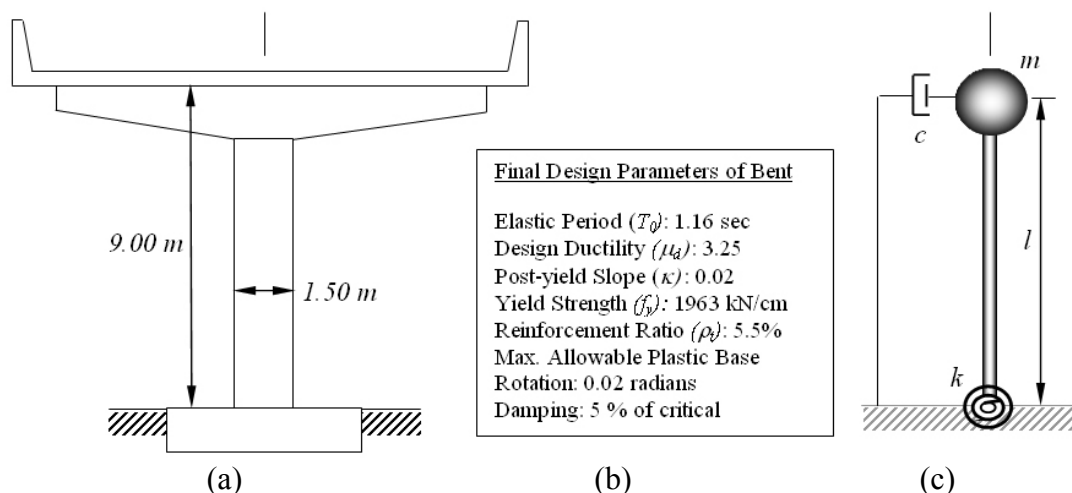


Fig. 10 (a) Single column of a bridge bent; (b) Design parameters; (c) Idealized SDOF system

Repeating the analysis by including the P-Δ effects (to be referred to as Case-2) escalates the ductility demand from 3.24 to 3.32. The difference is only 2.5 percent of the demand for Case-1. Thus, inclusion of the P-Δ effects for a long-length system excited by the translational motion only has limited impact on the peak displacement demand (although the system got pushed to almost 3 percent additional relative drift). The geometric-stiffness term contributes more to the overall stiffness, as the height of the system decreases, as opposed to an increase in the axial load. As compared to Case-2, when the horizontal component is coupled with the vertical component, the P-Δ effects gain more significance since vertical component starts playing role in the geometric-stiffness formulation (see Equation (8)). Figure 12 compares the results for the coupled horizontal and vertical components motion (to be referred to as Case-3) with those of the horizontal excitation with and without the P-Δ effects (i.e., Case-2 and Case-1, respectively). Coupling of the vertical component with the horizontal one essentially has no influence on the inertia force (see Equation (9)), and the normalized input force remains unchanged (see the right top panel in Figures 11 and 12); however influence of the vertical excitation on the geometric-stiffness term and consequently on the SDOF response is evident from the force-deformation relation and displacement time-history plots. Coupling of the horizontal and vertical components in this example raises the ductility demand to 3.63, which is 12 percent larger than the design level (i.e., Case-1). More importantly, the P-Δ effects enhanced by the vertical motion create negative tangent stiffness in the post-yield deformation range by offsetting the effects of kinematic strain hardening. As mentioned earlier this, in turn, can distort

the expected performance of the structure by causing the inelastic deformation accumulation in one direction.

In general, systematic differences between Case-1 and Case-3 show that the structure designed for horizontal component only, without accounting for the influence of vertical component coupling, may lead to non-conservatism. It should be also reminded that the inclusion of vertical component does not necessarily worsen the seismic demand. Depending on the phase difference between the major vertical acceleration pulses and the gravitational acceleration, the vertical component may act conversely and minimize the P- Δ effects.

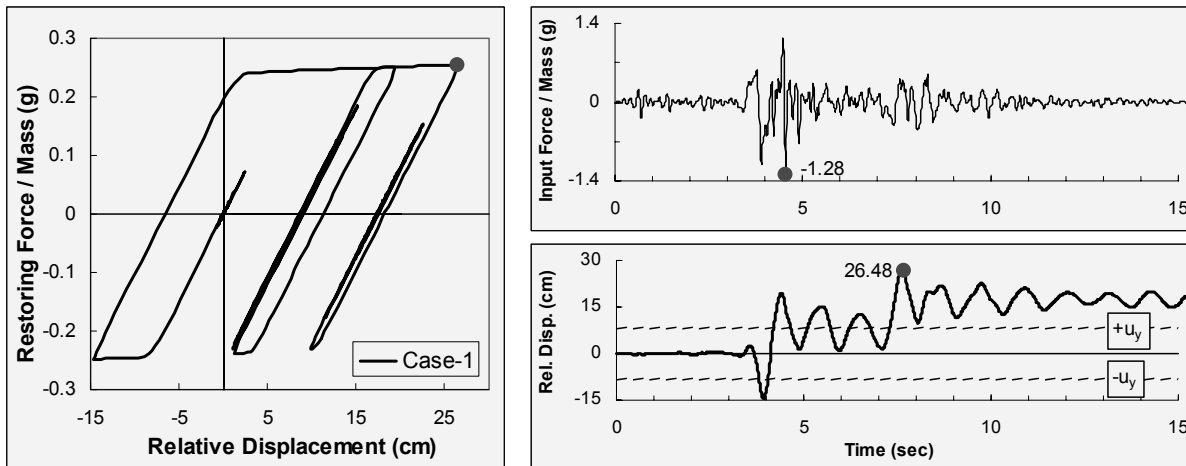


Fig. 11 Inelastic response of the idealized single bridge bent under the translation component of the Pacoima dam upper left abutment record (Case-1) (P- Δ effects are not included; filled circles (●) denote the peak values; dashed lines in the displacement time-history indicate the negative and positive yield-displacement demands)

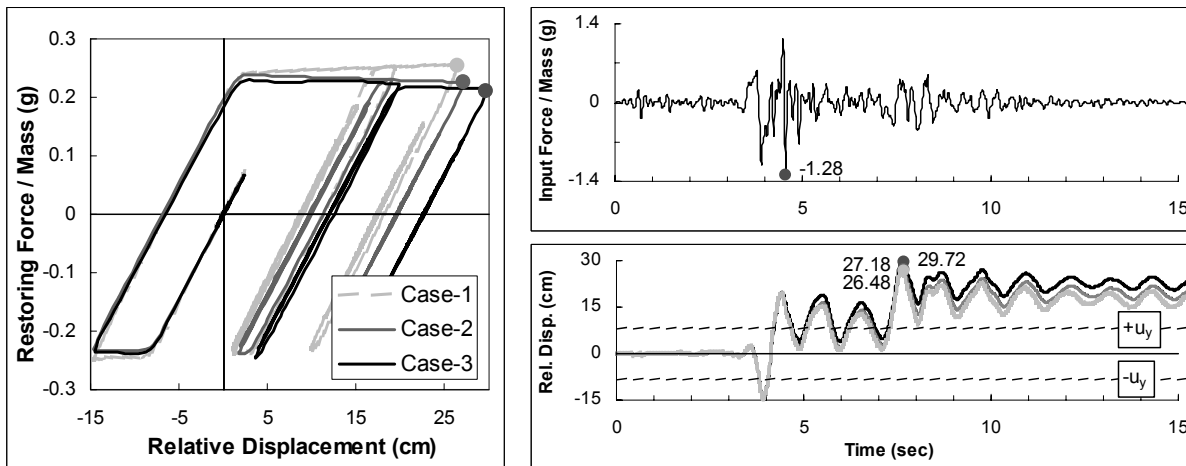


Fig. 12 Comparison of the force-deformation relations for various combinations of the horizontal and vertical components of ground motion and the P- Δ effects (Case-1: horizontal excitation without the P- Δ effects; Case-2: horizontal excitation with the P- Δ effects; Case-3: coupled horizontal and vertical excitations with the P- Δ effects)

In the example shown in Figure 12 (see Case-3), vertical pulses are seen to be in phase with the gravity; therefore, they tend to reduce the overall system stiffness by magnifying the geometric-stiffness term. The vertical component is next applied with opposite sign (to be referred to as Case-4), and corresponding response of the SDOF oscillator is compared in Figure 13(a) with that of Case-1, Case-2 and Case-3. Maximum ductility of the SDOF oscillator in Case-4 is limited to 3.0. Therefore, compared to Case-1 (i.e., the design case), the coupling of horizontal and vertical components either causes 8

percent reduction or 12 percent increase in the ductility demand, depending on the direction of the acceleration pulses contained in the vertical component of the motion. It is also important to observe that the vertical component progressively influences the overall stiffness of the system. Such behaviour manifests itself as distortions (due to the wave-effect) on the slope of the force-deformation relation, which is initially set as a smooth transition in the nonlinear material model (see the small window in Figure 13(b)); these distortions become more obvious as the ductility demand increases).

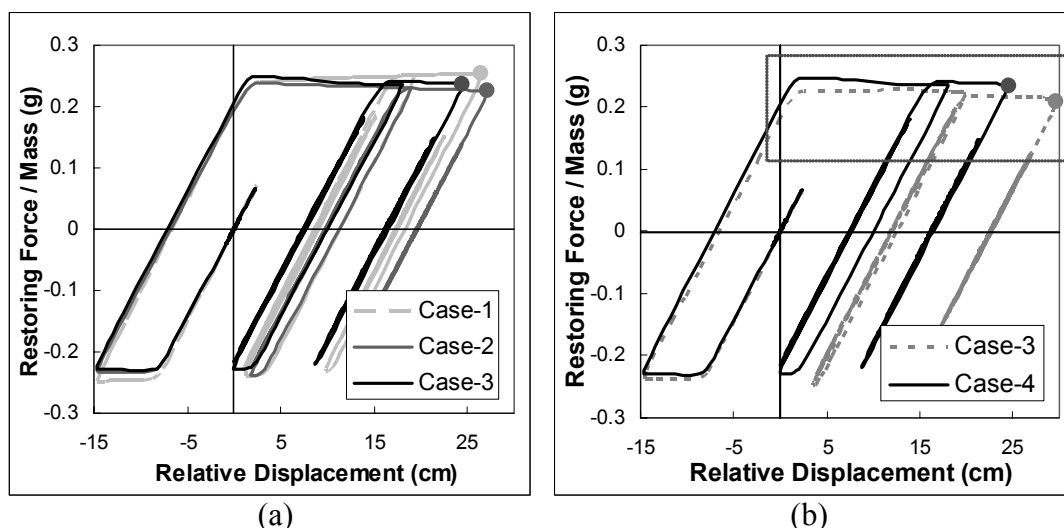


Fig. 13 Comparison of the force-deformation relations for various combinations of the horizontal and vertical components of ground motion and the P-Δ effects (Case-1: horizontal excitation without the P-Δ effects; Case-2: horizontal excitation with the P-Δ effects; Case-3: coupled horizontal and vertical excitations with the P-Δ effects)

So far, the impact of the simultaneous application of the vertical and horizontal components on the displacement and ductility demands of a bridge bent is comparatively demonstrated. In the next phase, the tilt component of the motion is incorporated in the response computations. Note that unlike the vertical motion, the tilt component affects the right side of the equation of motion by introducing additional lateral forces (see Equations (6) and (10)); yet it has no impact on the geometric-stiffness term. Figure 14 compares the inelastic displacement response of the SDOF oscillator when the three components are applied in tandem (to be referred to as Case-5). Also plotted in Figure 14 is the response from Case-3 for a direct comparison. It is evident that inclusion of the tilt motion during the response analysis results in a noticeable asymmetric deformation compared to the previous cases (Case-1 to Case-4). One of the consequences of the asymmetric deformation is a large relative displacement and the resultant higher ductility demand. The maximum ductility demand caused by the coupled motion extends to 9.1, while it remains only 3.63 when the tilt effects are excluded. Therefore, for the tall systems, the tilt component (if it reaches a few degrees) has a more pronounced impact than the vertical motion. Figure 14 suggests that the structures that would not have collapsed under a few cycles of shaking may be driven to collapse due to additional plastic cycles associated with the coupling of ground motion components (if $|\kappa-\theta|$ is large enough). In fact, coupling of the three components of motion results in numerous additional cycles of deformation that exceed the yield rotation. Since the inelastic response results in a permanent drift, it is more convenient to count the number of half-cycles wherein each half-cycle is the peak-to-peak amplitude. If the peak-to-peak amplitude exceeds twice the yield rotation, each such cycle is referred to as a “plastic cycle” (Kalkan and Kunnath, 2006). For Case-5, there were eight half-plastic cycles during the response, whereas ignoring tilt component as in Case-3 produced only three half-plastic cycles. The cumulative damage resulting from the plastic cycles in degrading systems (although not considered here) is much greater than that implied by the peak ductility demand and should not be ignored in the performance assessment of structural systems (Kunnath and Kalkan, 2004).

Another important aspect of including tilt in the analysis is the resultant maximum and residual base rotation from the design and serviceability point of view. Figure 15 compares the drift time-histories for the SDOF oscillator excited by multi-component motions (i.e., Case-5 and Case-3) and by the

translational motion alone (i.e., Case-1). Recall that the permissible column base rotation constraint by the design is 0.02 rad. Case-1 satisfies this design criterion by producing peak plastic rotation not exceeding but close to 0.02 rad. This limit is exceeded in Case-3 by 20 percent, whereas Case-5 exerts large influence on the drift demand with the system pushed to almost 8 percent plastic rotation. This is significantly (almost four times) larger than the design limit. There is also an obvious difference in the residual rotations in the coupled cases and in that caused by the translational motion alone. As the ground motion ceased, the SDOF oscillator excited by the translational component remained in the tilted position at only 0.7° (0.012 rad), while considering coupling of the three components doubled it in the opposite direction with a relative inclination of 1.4° (0.024 rad).

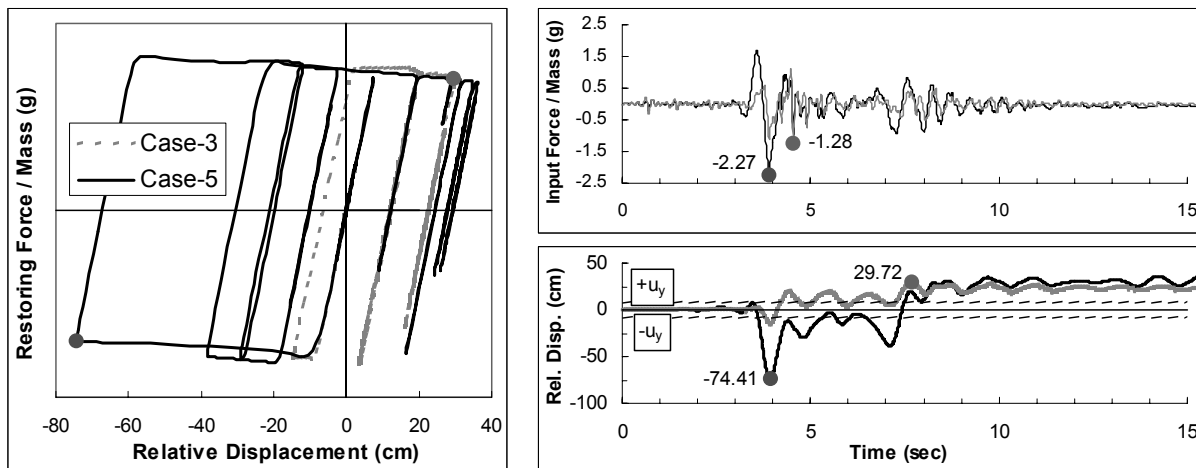


Fig. 14 Comparison of the force-deformation relations for various combinations of the horizontal and vertical components and the P-Δ effects (Case-3: coupled horizontal and vertical excitations with the P-Δ effects; Case-5: coupled horizontal, vertical and tilting excitations with the P-Δ effects)

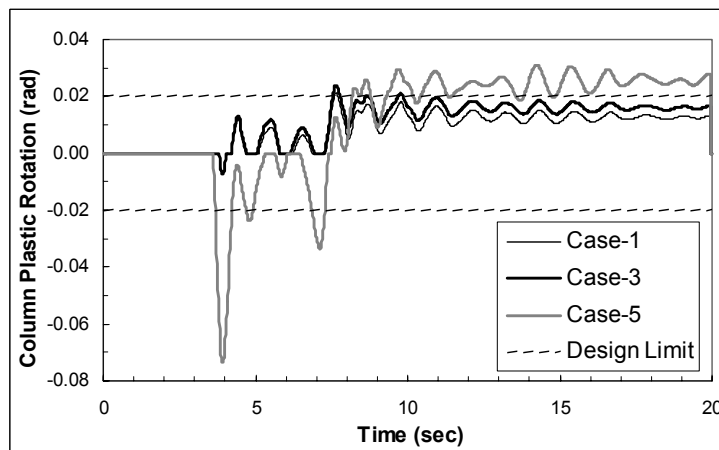


Fig. 15 Column plastic rotation demands imposed by the translational motion (Case-1), coupled translational and vertical motion (Case-3), and by the coupled translational, vertical and tilt motion (Case-5) (dashed lines indicate the permissible plastic rotation constraint by design)

Figures 14 and 15 collectively indicate that coupling of the three components leads to a radically different dynamic response as compared to the response produced by the horizontal motion alone. An eminent fact that emerges from these results is that if the maximum deformation demand is considered as a performance evaluation criterion, one neglects the big difference in the behavior that a system exhibits on considering or not considering the multi-component coupling effects. In order to systematically address this issue in the design of new structures or in the performance evaluation of existing structures, peak response values for a range of periods are computed and combined in a spectral format. The

resultant spectrum is referred to as “multi-component ground motion response spectrum”, and it is conceptually detailed in the following section.

MULTI-COMPONENT GROUND MOTION RESPONSE SPECTRA

For the design and performance assessment of structures, a ground motion spectrum is often computed considering only the horizontal component. In rare applications, the vertical ground motion spectrum is also utilized in parallel. In generating a horizontal spectrum, it is customary to characterize the P- Δ effects by the constant values of stability coefficient θ (e.g., Bernal, 1998; MacRae, 1994), although in many cases such effects are completely disregarded. As mentioned earlier, the use of θ in a spectral format is misleading since θ is a spectral-period-dependent parameter (see Equation (2)). On the other hand, the “geometric oscillation period” (T_G or T'_G) becomes a more meaningful descriptor to characterize the P- Δ effects since it is independent of the spectral period. For the bridge bent example shown in Figure 10, T_G equals 6.0 s, being much larger than $T_0 = 1.16$ s. The large difference between T_G and T_0 implies that instability is unlikely to occur as long as the system is subjected to the horizontal excitation alone. On the other hand, due to the vertical component coupling, geometric oscillation period becomes time-variant (see Equation (12)). Figure 16 shows the plot of the time-variation of T'_G when the vertical and horizontal components are simultaneously applied to the SDOF oscillator base. Also marked in this figure is the constant value of T_G as a reference to demonstrate the degree of fluctuation. Note that in the beginning and as the amplitude of the vertical component of motion diminishes, T'_G converges to T_G . Stability in the system increases as T'_G becomes larger than T_G . On the other hand, the system tends to be less stable if T'_G falls below T_G . As Figure 16 shows, the minimum value of T'_G is 4.04 s, being 30 percent smaller than T_G . If the vertical excitation effects are accounted for in the translational response computation, it is always recommended to check the variation of T'_G before starting the analysis or design process. For stable systems, T'_G should always be larger than T_0 (see Equation (14)); likewise θ' should be less than unity.

In order to identify those situations in which the overall response is likely to receive significant contributions from the vertical and tilt components of ground motion, regular response spectra (based on the translational motion only) and multi-component ground motion spectra including the three components of motion in tandem are compared. 5 percent of critical damping is used for each case, and three components of Pacoima dam record are used as the input. The P- Δ effects are represented by the “geometric oscillation period” ($T'_{G,\min} = 4.04$ s in the cases where the vertical excitation is accounted for). Figure 17 portrays the elastic (i.e., ductility = 1.0) and inelastic spectral response quantities of interest, i.e., the relative displacement of a SDOF system and its time derivatives. The inelastic spectra are generated for the constant ductility ratios of 3 and 6. As depicted, the tilt component, when it is coupled with the vertical and translational components, amplifies all response quantities regardless of the spectral period. The difference between the two cases becomes more pronounced as the spectral period increases, and is noticeable at all ductility levels. At the mid-range and longer periods, the multi-component excitation yields more than three times larger spectral displacement demand compared to the displacement demand imposed by the pure translational motion. The major contributor to the amplified seismic level is the tilt component whose adverse effects are inherently conditioned on the height of the system. Based on the difference between the spectral ordinates in Figure 17, it can be concluded that ground tilting of few degrees can be most detrimental, particularly for the long and flexible structures.

These results indicate that isolating the effects of vertical and horizontal excitations in design or assessment studies by ignoring their coupling effects could be misleading. Given a structural system and estimated yield displacement, the usual design process is to determine the associated strength value required to limit the ductility and peak displacement response within acceptable performance levels. In that respect, multi-component spectra can serve as a useful tool, since the multi-component excitation effects on the translational response of the system can be estimated accurately by using the information available in the early stage of design process (i.e., initial period, damping, and design ductility demand).

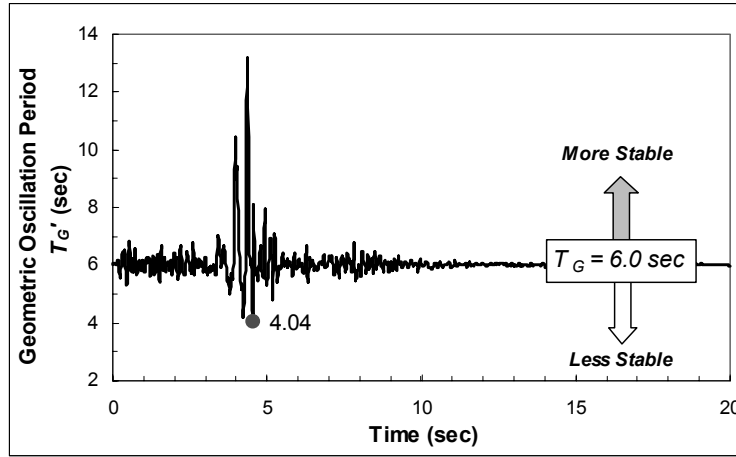


Fig. 16 Time variation of geometric oscillation period (T_G')

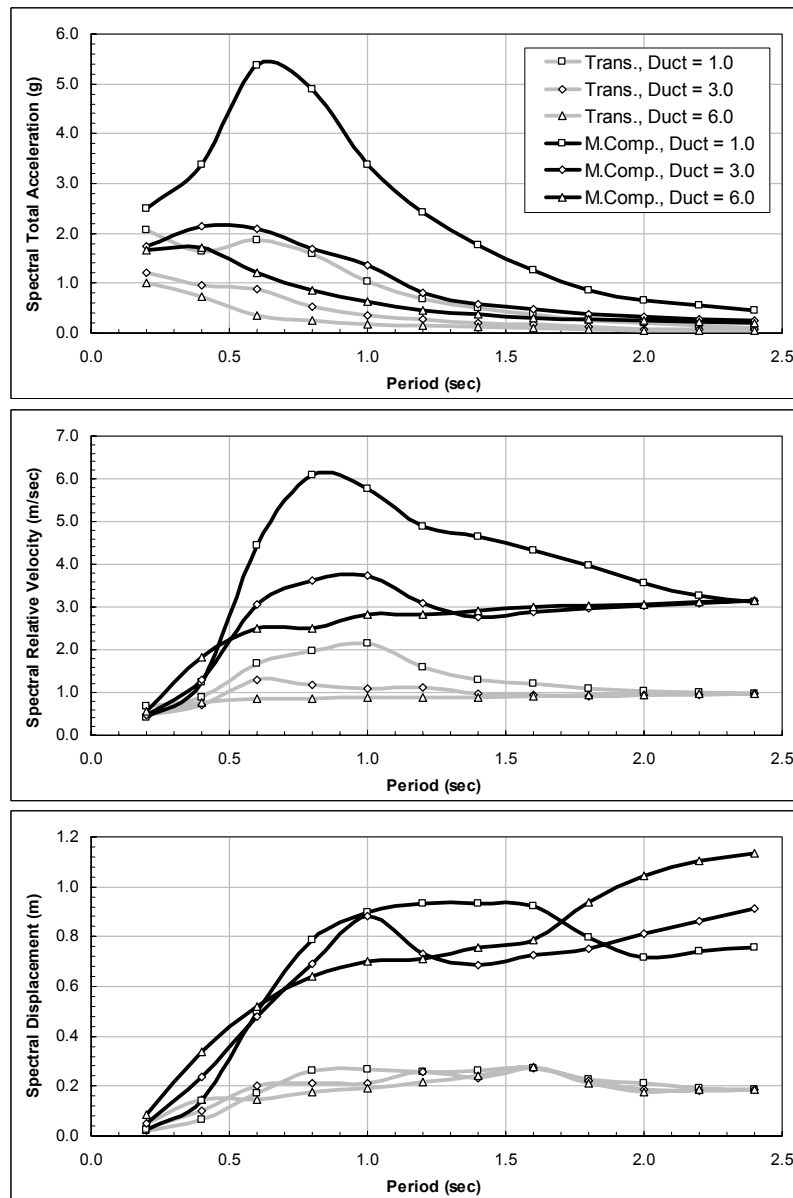


Fig. 17 Constant-ductility inelastic response spectra for acceleration, velocity and displacement (Trans.: translational motion only without the P- Δ effects; M. Comp.: multi-component excitation with the P- Δ effects)

SUMMARY AND CONCLUSIONS

In current practice, seismic demands are established based on the horizontal excitation through an uncoupled equation of motion without paying attention to the P- Δ effects. Vertical and rotational components on the other hand are almost always neglected. In reality, peak amplitude of the vertical ground motion can exceed that of the horizontal motion at short periods and near-source distances. Intensity of the rotational components may also be large in the near-field zone. For a structure to exhibit satisfactory performance, its seismic design should provide adequate stiffness and strength so that its ultimate ductility level does not exceed its maximum ductility under the design level seismic excitation. Using the above as a performance evaluation criterion, a structure exhibiting satisfactory seismic performance under a translational motion may go into large displacement demands (or even collapse) when the translational motion is coupled with intense vertical motion and/or ground tilting of a few degrees. In order to put such amplified seismic demands in proper design and performance assessment perspective, the governing equation of motion that implicitly constitutes the forcing functions associated with the multi-component excitations is postulated. The extended equation is theoretically complete for the three components of motion. Based on this equation, the multi-component spectrum is proposed for use in engineering applications. The proposed spectrum reflects the kinematic characteristics of the ground motion that are not identifiable by the conventional ground motion response spectrum alone, at least for the near-fault region where the high intensity vertical shaking and rotational excitation are likely to occur.

Based on the findings of this study, the following conclusions are made:

- Comparison of the coupled and uncoupled equations of motion used to compute the response of the SDOF oscillator clearly indicates the level of simplification that is introduced by ignoring the vertical component and the ground tilting. Results of the current work and our previous study (Kalkan and Graizer, 2007) emphasize that inclusion of vertical and tilt components in the computation of the ductility demand results in additional forcing functions and enhanced P- Δ effects. The resulting amplified seismic demand and eroded stiffness may adversely influence the displacement (ductility) demand and dynamic stability. Therefore, for structures susceptible to high-intensity vertical shaking and/or ground tilting, multi-components effects should be considered in their seismic design or performance assessment.
- Except in rare applications, P- Δ effects are practically neglected when the seismic demands are presented in a spectral format. The difference between the first-order and second-order analyses becomes evident, as the coupling of vertical and tilt components is included. In this respect, geometric-stiffness term turns out to be the controlling parameter. It is independent of both non-stationary tilting and horizontal excitations, whereas it is a function of axial load, vertical motion and length of the oscillator.
- If the direction of dominant vertical pulses is in phase with the gravity, they may diminish the overall stiffness of system by increasing the contribution of the geometric-stiffness term. The associated enhanced P- Δ effects may create negative tangent stiffness in the post-yield deformation range by offsetting the effects of kinematic strain hardening. Hence, the bias towards increasing displacements in one direction becomes increasingly larger. This may create important practical consequences, e.g., dynamic instability (or collapse) can be initiated if the energy of the multi-component excitations is large enough to carry the system inelastically in one direction. On the other hand, if the major pulses in the vertical component are out of phase with respect to the gravity, they act conversely and tend to minimize the destabilizing force. Same applies for the tilt component: depending upon its phase difference with respect to the horizontal motion, it may either remediate the system by offsetting the plastic rotations and reducing the overall inertia force, or it may act in line with the horizontal motion and amplify the total inertia force.
- Inclusion of tilt excitation in the dynamic response computations increases the individual forcing functions on the right side of the equation of motion, and its P- Δ contribution is implicitly considered within the geometric-stiffness term; therefore the only change takes place on the right side of the equation. However, including vertical component in addition to the tilt excitation results in not only an additional forcing term on the right side of the equation but also in a change on the left side of the equation within the geometric-stiffness term. The modified term becomes time-variant and vertical component may gradually modify its value. The instantaneous changes in the geometric-stiffness term

create progressive modifications in the overall stiffness. This situation can virtually be observed from the initial slope of the force-deformation curve, which may diverge, at any instant, from its initial linear elastic position (this divergence is even more pronounced in the inelastic regime). The intensity of these time-variant changes (referred to as the “wave-effect”) in the force-deformation slope depends on the amplitude of the vertical acceleration pulses. If the intensity of the vertical acceleration pulses is large enough, the oscillator period may show noticeable variations. In that case, it is not possible to retain a constant-period oscillation, and a linear-elastic oscillator may act as a nonlinear-elastic oscillator. This phenomenon may have unfavorable effects, especially on the inverted pendulums used in some old ground motion recording instruments (e.g., mechanical horizontal seismometer of Weichert).

- In this study, geometric oscillation period (T_G) (or T'_G if vertical excitation is considered) is used in lieu of the stability coefficient (θ), to represent the P- Δ effects in response spectra. Unlike the geometric oscillation period, θ is a function of the stiffness (i.e., spectral period); therefore, it cannot be a spectrum-compatible parameter (assuming that the length of the oscillator is kept invariant at each spectral period). For a stable system, geometric oscillation period should be greater than the initial elastic period. Therefore, T_G (or T'_G) can serve as a valuable tool in design to assure stability by quantifying the lower-bound limit for the lateral stiffness while considering possible intensity of the vertical shaking (to be on the conservative side, peak intensity of the vertical motion should be assumed to be in phase with the gravity).
- Compared to vertical component, tilt component of the motion has more impact on the translational response of the system. Few degrees of dynamic ground tilting can easily double the overall system response. This difference will be more pronounced for the tall structures since the inertia force due to the angular acceleration is directly proportional to the effective height.
- The governing equation of motion considering the multi-component excitation is derived based on the concept of equivalent fixed-base oscillator; hence it directly provides the relative drift associated with the exact deformation. This interpretation makes the implementation easy in a computational framework. In this study, the equations of motion were formulated in a state-space form in MATLAB, and were solved in time domain by using the stiff ordinary differential equation solver (ODE15s).

Formulations and methodology presented herein are limited to the structural systems that can be potentially idealized as a SDOF oscillator. The vertical oscillation of mass and its corresponding effects (i.e., axial force and bending moment interaction at the section level) were not accounted for. Expanding the analytical approach for including such effects requires the SDOF idealization to be violated and thus necessitates a MDOF system solution. Foundation effects and associated rocking response were also not included; readers are referred to the study by Kalkan and Graizer (2007) for including the rocking effects. Results presented here are based on three components (i.e., horizontal, vertical and tilt) of the Pacoima dam upper left abutment record. The physically measured permanent tilt at this station (few days after the earthquake) provided the opportunity to extract a realistic tilting motion. Due to the recorded rotational components during a strong ground shaking being unavailable, our results are limited to the ground motion recorded at this station only.

ACKNOWLEDGEMENTS

We would like to thank Dr. E. Erduran for compiling near-fault ground motion subset from the NGA dataset. Sincere thanks are extended to Professor M.D. Trifunac for his encouragement and valuable comments. We also acknowledge the suggestions of three anonymous reviewers, which improved the technical quality of the paper. Any opinions, findings, and conclusions or recommendations expressed in this paper are those of the authors solely and do not necessarily reflect the views of the California Geological Survey.

REFERENCES

1. Abdelkareem, K.H. and Machida, A. (2000). "Effects of Vertical Motion of Earthquake on Failure Mode and Ductility of RC Bridge Piers", Proceedings of the 12th World Conference on Earthquake Engineering, Auckland, New Zealand, Paper No. 0463 (on CD).
2. Akiyama, H. (1985). "Earthquake-Resistant Limit-State Design of Buildings", University of Tokyo Press, Tokyo, Japan.
3. Ambraseys, N.N. and Simpson, K.A. (1996). "Prediction of Vertical Response Spectra in Europe", Earthquake Engineering & Structural Dynamics, Vol. 25, No. 4, pp. 401–412.
4. Ariman, T. and Muleski, G.E. (1981). "A Review of the Response of Buried Pipelines under Seismic Excitation", Earthquake Engineering & Structural Dynamics, Vol. 9, No. 2, pp. 133–152.
5. Bernal, D. (1998). "Instability of Buildings during Seismic Response", Engineering Structures, Vol. 20, No. 4-6, pp. 496–502.
6. Biot, M.A. (1932). "Transient Oscillations in Elastic Systems", Ph.D. Thesis No. 259, Aeronautics Department, California Institute of Technology, Pasadena, U.S.A.
7. Biot, M.A. (1933). "Theory of Elastic Systems Vibrating under Transient Impulse with an Application to Earthquake-Proof Buildings", Proceedings of the National Academy of Sciences of the United States of America, Vol. 19, No. 2, pp. 262–268.
8. Biot, M.A. (1934). "Theory of Vibration of Buildings during Earthquake", Zeitschrift für Angewandte Mathematik und Mechanik, Vol. 14, No. 4, pp. 213–223.
9. Biot, M.A. (1941). "A Mechanical Analyzer for the Prediction of Earthquake Stresses", Bulletin of the Seismological Society of America, Vol. 31, No. 2, pp. 151–171.
10. Biot, M.A. (1942). "Analytical and Experimental Methods in Engineering Seismology", ASCE Transactions, Vol. 108, pp. 365–408.
11. Bouchon, M. and Aki, K. (1982). "Strain, Tilt, and Rotation Associated with Strong Ground Motion in the Vicinity of Earthquake Faults", Bulletin of the Seismological Society of America, Vol. 72, No. 5, pp. 1717–1738.
12. Bozorgnia, Y. and Campbell, K.W. (2004). "The Vertical-to-Horizontal Response Spectral Ratio and Tentative Procedures for Developing Simplified V/H and Vertical Design Spectra", Journal of Earthquake Engineering, Vol. 8, No. 2, pp. 175–207.
13. Bozorgnia, Y., Niazi, M. and Campbell, K.W. (1995). "Characteristics of Free-Field Vertical Ground Motion during the Northridge Earthquake", Earthquake Spectra, Vol. 11, No. 4, pp. 515–525.
14. Bycroft, G.N. (1980). "Soil-Foundation Interaction and Differential Ground Motions", Earthquake Engineering & Structural Dynamics, Vol. 8, No. 5, pp. 397–404.
15. Castellani, A. and Boffi, G. (1986). "Rotational Components of the Surface Ground Motion during an Earthquake", Earthquake Engineering & Structural Dynamics, Vol. 14, No. 5, pp. 751–767.
16. Chopra, A.K. (1966). "The Importance of the Vertical Component Earthquake Motions", Bulletin of the Seismological Society of America, Vol. 56, No. 5, pp. 1163–1175.
17. Chopra, A.K. and Goel, R.K. (2001). "Direct Displacement-Based Design: Use of Inelastic vs. Elastic Design Spectra", Earthquake Spectra, Vol. 17, No. 1, pp. 47–64.
18. Diotallevi, P.P. and Landi, L. (2000). "Effect of the Axial Force and of the Vertical Ground Motion Component on the Seismic Response of R/C Frames", Proceedings of the 12th World Conference on Earthquake Engineering, Auckland, New Zealand, Paper No. 1026 (on CD).
19. Elnashai, A.S. and Papazoglou, A.J. (1997). "Procedure and Spectra for Analysis of RC Structures Subjected to Strong Vertical Earthquake Loads", Journal of Earthquake Engineering, Vol. 1, No. 1, pp. 121–155.
20. Ghafory-Ashtiany, M. and Singh, M.P. (1986). "Structural Response for Six Correlated Earthquake Components", Earthquake Engineering & Structural Dynamics, Vol. 14, No. 1, pp. 103–119.
21. Graizer, V.M. (1987). "Determination of the Path of Ground Motion during Seismic Phenomena", Izvestiya, Physics of the Solid Earth, Vol. 22, No. 10, pp. 791–794.

22. Graizer, V.M. (1989). "Bearing on the Problem of Inertial Seismometry", *Izvestiya, Physics of the Solid Earth*, Vol. 25, No. 1, pp. 26–29.
23. Graizer, V.M. (1991). "Inertial Seismometry Methods", *Izvestiya, Physics of the Solid Earth*, Vol. 27, No. 1, pp. 51–61.
24. Graizer, V. (2006a). "Tilts in Strong Ground Motion", *Bulletin of the Seismological Society of America*, Vol. 96, No. 6, pp. 2090–2102.
25. Graizer, V. (2006b). "Comparison of Attenuation of Peak Ground Motion and V/H Ratios for California Earthquakes (Abstract)", *Seismological Research Letters*, Vol. 77, No. 2, p. 324.
26. Gupta, V.K. and Trifunac, M.D. (1990). "Response of Multistoried Buildings to Ground Translation and Torsion during Earthquakes", *European Earthquake Engineering*, Vol. IV, No. 1, pp. 34–42.
27. Gupta, V.K. and Trifunac, M.D. (1991). "Effects of Ground Rocking on Dynamic Response of Multistoried Buildings during Earthquakes", *Structural Engineering/Earthquake Engineering, JSCE*, Vol. 8, No. 2, pp. 87s–94s.
28. Hall, W.J., Mohraz, B. and Newmark, N.M. (1975). "Statistical Studies of Vertical and Horizontal Earthquake Spectra", Report NUREG-0003 (prepared for United States Nuclear Regulatory Commission), Newmark Consulting Engineering Services, Urbana, U.S.A.
29. Hart, G.C., Lew, M. and DiJulio, R.M. (1975). "Torsional Response of High-Rise Buildings", *Journal of the Structural Division, Proceedings of ASCE*, Vol. 101, No. ST2, pp. 397–414.
30. Housner, G.W. (1959). "Behavior of Structures during Earthquakes", *Journal of the Engineering Mechanics Division, Proceedings of ASCE*, Vol. 85, No. EM4, pp. 109–129.
31. Huang, B.S. (2003). "Ground Rotational Motions of the 1999 Chi-Chi, Taiwan Earthquake as Inferred from Dense Array Observations", *Geophysical Research Letters*, Vol. 30, No. 6, pp. 1307–1310.
32. Ishida, S. and Morisako, K. (1985). "Collapse of SDOF System to Harmonic Excitation", *Journal of Engineering Mechanics, ASCE*, Vol. 111, No. 3, pp. 431–448.
33. Jennings, P.C. and Husid, R. (1968). "Collapse of Yielding Structures during Earthquakes", *Journal of the Engineering Mechanics Division, Proceedings of ASCE*, Vol. 94, No. 5, pp. 1045–1065.
34. JSCE (1995). "Preliminary Report on the Great Hanshin Earthquake, January 17, 1995", Japan Society of Civil Engineers, Tokyo, Japan.
35. Kalkan, E. and Gülkan, P. (2004a). "Site-Dependent Spectra Derived from Ground Motion Records in Turkey", *Earthquake Spectra*, Vol. 20, No. 4, pp. 1111–1138.
36. Kalkan, E. and Gülkan, P. (2004b). "Empirical Attenuation Equations for Vertical Ground Motion in Turkey", *Earthquake Spectra*, Vol. 20, No. 3, pp. 853–882.
37. Kalkan, E. and Graizer, V. (2007). "Coupled Tilt and Translational Ground Motion Response Spectra", *Journal of Structural Engineering, ASCE*, Vol. 133, No. 5, pp. 609–619.
38. Kalkan, E. and Kunnath, S.K. (2006). "Effects of Fling Step and Forward Directivity on the Seismic Response of Buildings", *Earthquake Spectra*, Vol. 22, No. 2, pp. 367–390.
39. Kharin, D.A. and Simonov, L.I. (1969). "VBPP Seismometer for Separate Registration of Translational Motion and Rotations", *Seismic Instruments*, Vol. 5, pp. 51–66 (in Russian).
40. Kunnath, S.K. and Kalkan, E. (2004). "Evaluation of Seismic Deformation Demands Using Non-linear Procedures in Multistory Steel and Concrete Moment Frames", *ISET Journal of Earthquake Technology*, Vol. 41, No. 1, pp. 159–181.
41. Kunnath, S., Abrahamson, N., Chai, Y.H., Zong, Z. and Yilmaz, Z. (2005). "Effects of Vertical Ground Motions on Seismic Response of Highway Bridges", *Proceedings of the Bridge Research Conference 2005, Sacramento, U.S.A., Paper No. 02-504 (on CD)*.
42. Lam, N., Wilson, J., Chandler, A. and Hutchinson, G. (2000). "Response Spectrum Modeling for Rock Sites in Low and Moderate Seismicity Regions Combining Velocity, Displacement and Acceleration Predictions", *Earthquake Engineering & Structural Dynamics*, Vol. 29, No. 10, pp. 1491–1525.
43. Lee, V.W. (1979). "Investigation of Three-Dimensional Soil-Structure Interaction", Report CE 79-11, University of Southern California, Los Angeles, U.S.A.

44. Lee, V.W. and Trifunac, M.D. (1985). "Torsional Accelerograms", *International Journal of Soil Dynamics and Earthquake Engineering*, Vol. 4, No. 3, pp. 132–139.
45. Lee, V.W. and Trifunac, M.D. (1987). "Rocking Strong Earthquake Accelerations", *Soil Dynamics and Earthquake Engineering*, Vol. 6, No. 2, pp. 75–89.
46. MacRae, G.A. (1994). "P- Δ Effects on Single-Degree-of-Freedom Structures in Earthquakes", *Earthquake Spectra*, Vol. 10, No. 3, pp. 539–568.
47. Malhotra, P.K. (2006). "Smooth Spectra of Horizontal and Vertical Ground Motions", *Bulletin of the Seismological Society of America*, Vol. 96, No. 2, pp. 506–518.
48. Mohraz, B. (1976). "A Study of Earthquake Response Spectra for Different Geological Conditions", *Bulletin of the Seismological Society of America*, Vol. 66, No. 3, pp. 915–935.
49. Newmark, N.M. and Hall, W.J. (1969). "Seismic Design Criteria for Nuclear Reactor Facilities", *Proceedings of the Fourth World Conference on Earthquake Engineering*, Santiago, Chile, Vol. B-4, pp. 37–50.
50. Newmark, N.M. and Hall, W.J. (1982). "Earthquake Spectra and Design", Monograph MNO-3, Earthquake Engineering Research Institute, Berkeley, U.S.A.
51. Newmark, N.M., Blume, J.A. and Kapur, K.K. (1973). "Seismic Design Spectra for Nuclear Power Plants", *Journal of the Power Division, Proceedings of ASCE*, Vol. 99, No. PO2, pp. 287–303.
52. Niazi, M. (1986). "Inferred Displacements, Velocities and Rotations of a Long Rigid Foundation Located at El Centro Differential Array Site during the 1979 Imperial Valley, California, Earthquake", *Earthquake Engineering & Structural Dynamics*, Vol. 14, No. 4, pp. 531–542.
53. Niazi, M. and Bozorgnia, Y. (1991). "Behavior of Near-Source Peak Horizontal and Vertical Ground Motions over SMART-1 Array, Taiwan", *Bulletin of the Seismological Society of America*, Vol. 81, No. 3, pp. 715–732.
54. Nigbor, R.L. (1994). "Six-Degree-of-Freedom Ground-Motion Measurement", *Bulletin of the Seismological Society of America*, Vol. 84, No. 5, pp. 1665–1669.
55. Oliveira, C.S. and Bolt, B.A. (1989). "Rotational Components of Surface Strong Ground Motion", *Earthquake Engineering & Structural Dynamics*, Vol. 18, No. 4, pp. 517–526.
56. Ozdemir, H. (1976). "Nonlinear Transient Dynamic Analysis of Yielding Structures", Ph.D. Dissertation, Department of Civil Engineering, University of California, Berkeley, U.S.A.
57. Pamuk, A., Kalkan, E. and Ling, H.I. (2005). "Structural and Geotechnical Impacts of Surface Rupture on Highway Structures during Recent Earthquakes in Turkey", *Soil Dynamics and Earthquake Engineering*, Vol. 25, No. 7-10, pp. 581–589.
58. Papazoglou, A.J. and Elnashai, A.S. (1996). "Analytical and Field Evidence of the Damaging Effect of Vertical Earthquake Ground Motion", *Earthquake Engineering & Structural Dynamics*, Vol. 25, No. 10, pp. 1109–1137.
59. Power, M., Chiou, B., Abrahamson, N. and Roblee, C. (2006). "The Next Generation of Ground Motion Attenuation Models (NGA) Project: An Overview", *Proceedings of the Eighth U.S. National Conference on Earthquake Engineering (8NCEE)*, San Francisco, U.S.A., Paper No. 2022 (on CD).
60. Ranzo, G., Petrangeli, M. and Pinto, P.E. (1999). "Vertical Oscillations due to Axial-Bending Coupling during Seismic Response of RC Bridge Piers", *Earthquake Engineering & Structural Dynamics*, Vol. 28, No. 12, pp. 1685–1704.
61. Salazar, A.R. and Haldar, A. (2000). "Structural Responses Considering the Vertical Component of Earthquakes", *Computers & Structures*, Vol. 74, No. 2, pp. 131–145.
62. Seed, H.B., Ugas, C. and Lysmer, J. (1976). "Site-Dependent Spectra for Earthquake-Resistant Design", *Bulletin of the Seismological Society of America*, Vol. 66, No. 1, pp. 221–243.
63. Shakal, A., Cao, T. and Darragh, R. (1994). "Processing of the Upper Left Abutment Record from Pacoima Dam for the Northridge Earthquake", Report OSMS 94-13, Department of Conservation, State of California, Sacramento, U.S.A.
64. Silva, W. (1997). "Characteristics of Vertical Strong Ground Motions for Applications to Engineering Design", *Proceedings of the Workshop on National Representation of Seismic Ground Motion for New and Existing Highway Facilities*, Burlingame, U.S.A., pp. 205–252.

65. Stratta, J.L. and Griswold, T.F. (1976). "Rotation of Footings due to Surface Waves", *Bulletin of the Seismological Society of America*, Vol. 66, No. 1, pp. 105–108.
66. Sun, C.-K., Berg, G.V. and Hanson, R.D. (1973). "Gravity Effect on Single-Degree Inelastic System", *Journal of the Engineering Mechanics Division, Proceedings of ASCE*, Vol. 99, No. EM1, pp. 183–200.
67. Takeo, M. and Ito, H.M. (1997). "What Can Be Learned from Rotational Motions Excited by Earthquakes?", *Geophysical Journal International*, Vol. 129, No. 2, pp. 319–329.
68. Trifunac, M.D. and Hudson, D.E. (1971). "Analysis of the Pacoima Dam Accelerogram—San Fernando, California, Earthquake of 1971", *Bulletin of the Seismological Society of America*, Vol. 61, No. 5, pp. 1393–1411.
69. Trifunac, M.D. and Todorovska, M.I. (1998). "Nonlinear Soil Response as a Natural Passive Isolation Mechanism—The 1994 Northridge, California, Earthquake", *Soil Dynamics and Earthquake Engineering*, Vol. 17, No. 1, pp. 41–51.
70. Trifunac, M.D., Todorovska, M.I. and Ivanović, S.S. (1996). "Peak Velocities and Peak Surface Strains during Northridge, California, Earthquake of 17 January 1994", *Soil Dynamics and Earthquake Engineering*, Vol. 15, No. 5, pp. 301–310.
71. Uenishi, K. and Sakurai, S. (2000). "Characteristic of the Vertical Seismic Waves Associated with the 1995 Hyogo-Ken Nanbu (Kobe), Japan Earthquake Estimated from the Failure of the Daikai Underground Station", *Earthquake Engineering & Structural Dynamics*, Vol. 29, No. 6, pp. 813–821.
72. Weichert, D.H., Wetmiller, R.J. and Munro, P. (1986). "Vertical Earthquake Acceleration Exceeding 2 g? The Case of the Missing Peak", *Bulletin of the Seismological Society of America*, Vol. 76, No. 5, pp. 1473–1478.